SAND REPORT

SAND2004-0670
Unlimited Release
Printed February 2004

The Effects of Varying Humidity on Copper Sulfide Film Formation

John P. Sullivan, J. Charles Barbour, Nancy A. Missert, R. Guild Copeland, Thomas M. Mayer, and Michael J. Campin

Prepared by
Sandia National Laboratories
Albuquerque, New Mexico 87185 and Livermore, California 94550

Sandia is a multiprogram laboratory operated by Sandia Corporation,
a Lockheed Martin Company, for the United States Department of
Energy under Contract DE-AC04-94AL85000.

Approved for public release; further dissemination unlimited.

Issued by Sandia National Laboratories, operated for the United States Department of Energy by Sandia Corporation.

NOTICE: This report was prepared as an account of work sponsored by an agency of the United States Government. Neither the United States Government, nor any agency thereof, nor any of their employees, nor any of their contractors, subcontractors, or their employees, make any warranty, express or implied, or assume any legal liability or responsibility for the accuracy, completeness, or usefulness of any information, apparatus, product, or process disclosed, or represent that its use would not infringe privately owned rights. Reference herein to any specific commercial product, process, or service by trade name, trademark, manufacturer, or otherwise, does not necessarily constitute or imply its endorsement, recommendation, or favoring by the United States Government, any agency thereof, or any of their contractors or subcontractors. The views and opinions expressed herein do not necessarily state or reflect those of the United States Government, any agency thereof, or any of their contractors.

Printed in the United States of America. This report has been reproduced directly from the best available copy.

Available to DOE and DOE contractors from
U.S. Department of Energy
Office of Scientific and Technical Information
P.O. Box 62
Oak Ridge, TN 37831

Telephone: (865)576-8401
Facsimile: (865)576-5728
E-Mail: reports@adonis.osti.gov
Online ordering: http://www.doe.gov/bridge

Available to the public from
U.S. Department of Commerce
National Technical Information Service
5285 Port Royal Rd
Springfield, VA 22161

Telephone: (800)553-6847
Facsimile: (703)605-6900
E-Mail: orders@ntis.fedworld.gov
Online order: http://www.ntis.gov/ordering.htm

SAND2004-0670
Unlimited Release
Printed February 2004

The Effects of Varying Humidity on Copper Sulfide Film Formation

John P. Sullivan, J. Charles Barbour, Nancy A. Missert, and R. Guild Copeland
Nanostructure and Semiconductor Physics Department

Thomas M. Mayer
Thin Film, Vacuum and Packaging Department

Sandia National Laboratories
P.O. Box 5800
Albuquerque, NM 87185

and

Michael J. Campin
International Sematech
Austin, TX 78741

Abstract

Detailed experiments involving extensive high resolution transmission electron microscopy (TEM) revealed significant microstructural differences between Cu sulfides formed at low and high relative humidity (RH). It was known from prior experiments that the sulfide grows linearly with time at low RH up to a sulfide thickness approaching or exceeding one micron, while the sulfide initially grows linearly with time at high RH then becomes sub-linear at a sulfide thickness less than about 0.2 microns, with the sulfidation rate eventually approaching zero. TEM measurements of the Cu_2S morphology revealed that the Cu_2S formed at low RH has large sized grains (75 to greater than 150 nm) that are columnar in structure with sharp, abrupt grain boundaries. In contrast, the Cu_2S formed at high RH has small equiaxed grains of 20 to 50 nm in size. Importantly, the small grains formed at high RH have highly disordered grain boundaries with a high concentration of nano-voids. Two-dimensional diffusion modeling was performed to determine whether the existence of localized source terms at the Cu/Cu_2S interface could be responsible for the suppression of Cu sulfidation at long times at high RH. The models indicated that the existence of static localized source terms would not predict the complete suppression of growth that was observed. Instead, the models suggest that the diffusion of Cu through Cu_2S becomes restricted during Cu_2S formation at high RH. The leading speculation is that the extensive voiding that exists at grain boundaries in this material greatly reduces the flux of Cu between grains, leading to a reduction in the rate of sulfide film formation. These experiments provide an approach for adding microstructural information to Cu sulfidation rate computer models. In addition to the microstructural studies, new micro-patterned test structures

were developed in this LDRD to offer insight into the point defect structure of Cu_2S and to permit measurement of surface reaction rates during Cu sulfidation. The surface reaction rate was measured by creating micropatterned Cu lines of widths ranging from 5 microns to 100 microns. When sulfidized, the edges of the Cu lines show greater sulfidation than the center, an effect known as microloading. Measurement of the sulfidation profile enables an estimate of the ratio of the diffusivity of H_2S in the gas phase to the surface reaction rate constant, k. Our measurements indicated that the gas phase diffusivity exceeds k by more than 10, but less than 100. This is consistent with computer simulations of the sulfidation process. Other electrical test structures were developed to measure the electrical conductivity of Cu_2S that forms on Cu. This information can be used to determine relative vacancy concentrations in the Cu_2S layer as a function of RH. The test structures involved micropatterned Cu disks and thin films, and the initial measurements showed that the electrical approach is feasible for point defect studies in Cu_2S.

CONTENTS

1.0 Introduction 5

2.0 Background on Copper Sulfidation 6

3.0 Initial Stages of Sulfidation 8

3.1 Water Adsorption 8

3.2 Nucleation 10

3.3 Stage I Kinetics 11

4.0 Micro-patterned Test Structures for Sulfidation 13

4.1 Background 13

4.2 Micro-loading Test Structures 15

4.3 Electrical Conductivity Test Structures 18

5.0 Microstructural Characterization of Copper Sulfide 22

5.1 Phase Identification of Copper Sulfide 22

5.2 SEM Surface Characterization 24

5.3 TEM Microstructure Characterization 25

6.0 Diffusion Modeling 29

7.0 Summary 31

8.0 Acknowledgments 32

9.0 References 32

1.0 Introduction

This report summarizes work performed under a laboratory directed research and development (LDRD) project on the effect of humidity on the atmospheric sulfidation of copper. Atmospheric corrosion of electrical components has been linked to a number of materials-related significant finding investigations (SFIs) for the nuclear weapons stockpile. Further, the increasing use of Cu in commercial systems will require a long-term commitment to understand Cu corrosion mechanisms in order to reliably predict corrosion rates for commercial off-the-shelf (COTS) discrete components in the future stockpile. This LDRD focused on the effects of varying relative humidity (RH) in the sulfidation of copper - a demonstrated and recurring corrosion problem for electrical devices.

The primary corrosion product that forms when Cu metal is sulfidized in an atmosphere containing $H_2S_{(g)}$ is Cu_2S, which is a semiconductor of modest electrical conductivity. Long term sulfidation has been known to lead to lateral overgrowth of Cu_2S, even to be point of bridging across insulating surfaces. This can give rise to an electrical leakage path that may short out an active device, and this failure mode has, in fact, been observed in discrete diode components that have been in long term storage.

A more common electrical fault is associated with Au-plated Cu connectors. Pinholes in the Au overcoat permit sulfidation of the underlying Cu when the connector is exposed to an environment containing sulfur. This can result in a bloom of Cu_2S that prevents intimate contact between the connector mating surfaces (see Fig. 1), leading to a large, and in some cases, unacceptable contact resistance. In order to effectively deal with these electrical component aging issues, the need – and the major challenge – is to be able to predict the growth rate and the morphology of the Cu_2S as a function of time and major environmental variables, such as $H_2S_{(g)}$ concentration and RH.

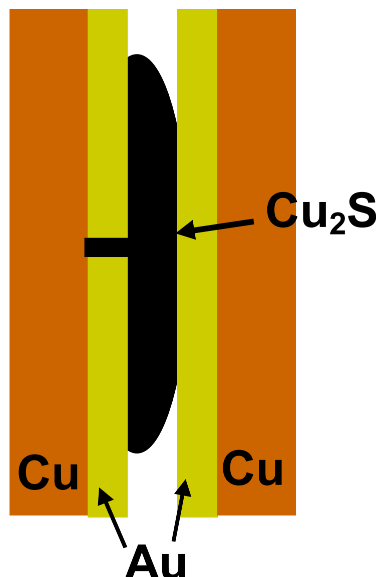

Fig. 1. Schematic of the problem of copper sulfidation at Au-plated Cu connectors. Sulfidation prevents intimate contact of the mating surfaces of the connector, leading to high electrical resistance across the connector.

2.0 Background on Copper Sulfidation

Copper is widely used in a number of critical electrical applications, and the problem and study of copper corrosion is a major area of research [1-8]. Previous researchers have studied the sulfidation of copper using SO_2 and H_2S gas and found that these reactants interact at the water-oxide interface, possibly at copper oxide grain boundaries [5,9-10]. Solid-state diffusion of copper through Cu_2O is thought to control the nucleation and initial Cu_2S island growth on Cu_2O – in the case of exposure to H_2S gas – and copper-sulfite and copper-sulfate formation – in the case of exposure to SO_2 gas [5-6]. Also, for both H_2S and SO_2 exposure, the rate of sulfidation can be controlled by the supply of corroding gas to the surface [4-5,11-12]. Beyond these few similarities, copper sulfidation by SO_2 and H_2S are very different. This study is focused on atmospheric sulfidation by H_2S.

Previous research indicated that the H_2S-induced copper sulfidation at moderate to high RH (RH>50%) occurs in two distinct stages, with Cu_2S as the main corrosion product formed [4,6,7,13]. In stage I of copper sulfidation, the sulfide grows linearly with time. In this stage, the thin islands of copper sulfide that initially form eventually grow laterally and coalesce, forming a uniform, porous film [4]. This layer then grows to a certain thickness, beyond which the rate of sulfide growth decreases [4,7]. This region is referred to as stage II. The literature generally indicates that the growth rate in stage II is proportional to $t^{1/2}$, suggestive of solid-state diffusion limited growth; however, we observe that the growth rate becomes much slower than $t^{1/2}$ and actually approaches zero for long times.

In case of sulfidation due to $H_2S_{(g)}$ exposure, a series of chemical reactions occurs when Cu metal is exposed to an oxidizing environment containing $H_2S_{(g)}$. Initially, the freshly-exposed Cu surface reacts with atmospheric oxygen to produce cuprous oxide, Cu_2O,

$$4Cu + O_{2(g)} \rightarrow 2Cu_2O_{(s)}. \quad (1)$$

In the presence of $H_2S_{(g)}$, it is favorable for a sulfidation reaction to proceed that results in the formation of cuprous sulfide, Cu_2S,

$$4Cu + 2H_2S + O_2 \rightarrow 2Cu_2S_{(s)} + 2H_2O. \quad (2)$$

In this reaction, the oxygen is reduced and H_2O is a byproduct. The reaction as written in (2) is an oversimplification of the complete sulfidation process, however. In detail, a number of reaction steps occur that lead up to the formation of the Cu_2S corrosion product. Many of these steps are outlined in the GILDES model of Graedel *et al.* [1,13]. One of the key steps in the sequence is the diffusion of Cu^0 through the surface oxide layer – and any existing Cu_2S that may be present – up to the sulfide-environment boundary. From prior experiments that we have performed, it was found that Cu is the primary diffuser in this system [14]. In an environment of high RH, an adsorbed H_2O layer up to a few monolayers thick is present on the sulfide surface. $H_2S_{(g)}$ may dissolve in this adsorbed H_2O layer and dissociate into a number of possible ionic species, e.g. $HS^-_{(aq)}$, $S^{2-}_{(aq)}$, $H^+_{(aq)}$. $O_{2(g)}$ will also dissolve in the adsorbed H_2O layer, providing the necessary oxidizing species for the sulfidation reaction. The rate of the Cu_2S formation will, therefore, depend on the rate at which H_2S can be supplied to the surface, the rate at which Cu is able to diffuse through the solid corrosion product layers, and the rates of the chemical reactions

at the sulfide surface or in the adsorbed H_2O layer (for example, the rates of the Cu + S reaction, the rates of the dissociation reactions, etc.).

One of the predictions of the GILDES model is that the adsorbed H_2O layer is critical to ensure a high rate of Cu sulfidation, i.e. the sulfidation rate at low RH would be less than that at high RH. In contrast to this expectation, however, early studies at Sandia showed that the sulfidation rate is not reduced at low RH, even at RH levels low enough that no condensed H_2O phase is expected on the Cu surface, see Fig. 2. What was perhaps more remarkable was that at long sulfidation times, the sulfidation rate remained constant at the initial value for experiments at low RH, while the sulfidation rate at high RH decreased with time and approached zero. Therefore, at long times, the sulfidation rate is observed to be *higher* at low RH than at high RH, in stark contrast to the expected behavior. This unexpected behavior is what prompted this study to identify the mechanism behind the effect of RH on the Cu sulfidation rate.

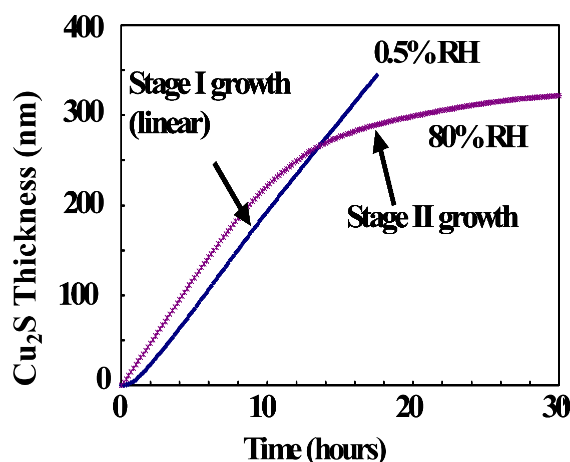

Fig .2. The observed sulfidation thickness vs. time for sulfidation of Cu at low RH and high RH in 160 ppb H_2S at 25°C. During the initial stages of sulfidation, the sulfide grows at a linear rate: Cu_2S thickness $\propto$ time. At longer time, the growth rate remains the same (up to microns in thickness) for sulfidation at low RH, while the rate decreases for sulfidation at high RH: Cu_2S thickness $\propto$ time$^{\alpha}$, with $\alpha < 1$ and α approaching 0 at long time.

For the experimental investigation of Cu sulfidation in this study, the sulfidation of both bulk Cu disks and copper thin films was investigated. However, copper thin films were used almost exclusively for transmission electron microscopy (TEM) analysis due to the ease of mechanical polishing techniques. To make the Cu thin film samples, copper was first electron-beam evaporated onto Ti-coated Si(100) wafers in ultra-high vacuum (UHV). The thin film copper was then sulfidized in a direct-impingement reactor, described below, at 15°C – 35°C and at 0.5% to 80% RH. The main difference between the two types of samples is that the copper thin films have much smaller grain size (~10-100 nm) than the bulk copper (~1 µm). However our previous work has shown that the sulfidation rate is similar for both types of samples.

Although not universally true, experience with our systems has shown that when copper metallization features corrode, they typically are sulfidized to form Cu_2S [15]. This, coupled with the fact that copper exposed to H_2S gas forms a Cu_2S product layer, led to our decision to

use H_2S as the corroding gas species in air with varying humidity levels to study copper corrosion in a well-controlled manner [4-6]. The corrosive environment reactor we chose to use provides well-defined, uniform flow conditions and minimizes the potential for gas-phase mass transport control. It is designed such that the change in the concentrations of H_2S, H_2O, and O_2, which occurs due to the depletion by corrosion mechanisms, is measured in the downstream gas environment. This allows us to measure the copper sulfidation as a function of chemical environment.

For the sulfidation of Cu, the $H_2S_{(g)}$ at ppb levels was supplied by a permeation tube and the inlet and outlet concentration of $H_2S_{(g)}$ was monitored continuously, along with the RH and temperature. Based upon the concentration of $H_2S_{(g)}$ supplied by the permeation tube and the flow rate, the thickness of Cu_2S formed at any point was calculated assuming a uniform, fully dense Cu_2S layer of density 5.6 g/cm^3. To control the RH, air at 100% RH was mixed with purified dry air. This air was subsequently mixed with a gas stream containing the H_2S gas. The resulting stream was then fed into the inlet of the sulfidation chamber at a constant flow rate of 1000 sccm. It should be noted that although the H_2S concentration in our reactor (~150-200 ppb) is small, it is significantly higher than the low ppb levels found in most environments [16,17]. Thus, our experiments represent accelerated aging of materials.

The H_2S gas concentration was measured by a gas analyzer at both the inlet and the outlet and was held constant to within ±1 ppb. To control the temperature over long periods of time (10s of hours), the entire reactor was placed in a refrigerator/oven with digital thermostat, which kept the temperature within the range 0°C – 40°C and within ±0.1°C of the target value. Measurements of the inlet and outlet H_2S gas concentration, the temperature, the RH, and flow rate were measured continuously at 2-minute intervals for the duration of the sulfidation exposure and saved in a Microsoft Excel spreadsheet for later analysis.

3.0 Initial Stages of Sulfidation

Differences in the long term sulfidation of Cu at low and high RH may be a direct result of differences in the earliest stages of sulfidation of Cu. (In this section and those that follow, we will define low RH to be equal to 0.5% RH and high RH to be equal to 80% RH.) The initial stages of sulfidation at low and high RH are influenced by the presence or absence of an adsorbed H_2O layer at the surface of the Cu, by the morphology and characteristics of the initial Cu_2S nuclei that form, and the kinetics that govern the initial sulfide growth. In order to address these issues, we examined the characteristics of water adsorption – a prelude to sulfidation – on the Cu_2O-coated Cu surface, the morphology of the initial Cu_2S nuclei, and the temperature dependence of the initial sulfidation reactions, all as a function of RH.

3.1 Water Adsorption

The characteristics of H_2O adsorption on a Cu_2O-covered Cu surface were examined using spectroscopic ellipsometry in an environmental chamber that permitted control of RH with an ambient background of $N_{2(g)}$. Figure 3 shows a schematic of the experimental geometry. The sample was prepared from a Cu thin film that was thermally evaporated on to a oxide-covered Si wafer. The surface of the Cu was allowed to oxidize upon exposure to air, producing a thin, approx. 1 to 10 nm thick, Cu_2O surface layer.

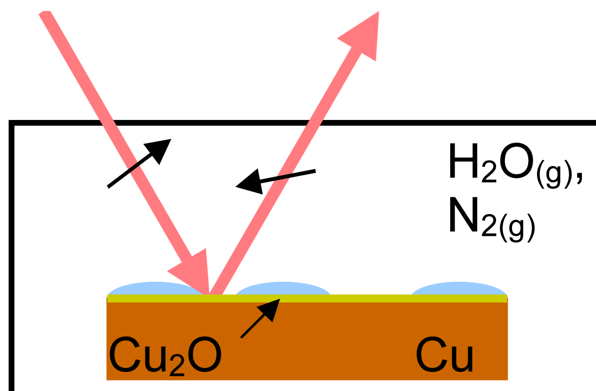

Fig. 3. Schematic of the ellipsometry measurement. The intensity and polarization of light reflected from a sample inside an environmentally-controlled chamber is measured as a function of RH.

It was expected that the primary difference that results from exposure to high and low RH would be the amount of adsorbed H_2O that exists at the sample surface. To investigate this process, we looked at the effect of water adsorption over the RH range from 20% to 80% (this particular system does not permit examination of surfaces at "low RH" = 0.5%). The ellipsometric measurements are sensitive to both the thickness of the adsorbed water layer (averaged over the illumination spot, which is < 1 mm^2), and the optical properties, e.g. refractive index, of the water layer + Cu_2O layer. The striking conclusion from these measurements was that there is very little increase in thickness of the adsorbed H_2O layer that forms on Cu_2O with increasing RH, but there is an increase in the polarizability of the Cu_2O layer, which is reflected as an increase in refractive index, see Fig. 4. Specifically, the H_2O causes chemical changes in the Cu_2O layer, possibly the formation of Cu-OH phases. One speculation of the effect this process may have on sulfidation is that the conversion of Cu_2O to $Cu(OH)_x$ may permit the solvation of Cu, i.e. the formation of $Cu^+_{(aq)}$ ions in solution. This suggests the possibility that sulfidation at high RH might occur by reaction of solvated Cu^+ and S^{2-} to form precipitating Cu_2S, which nucleates at the sample surface. This precipitation process would be expected to have a lower activation energy than the direct surface reaction involving adsorbed S reacting with $Cu_{(s)}$, which is expected to dominate at low RH. This speculation is supported by the measurements of the stage I kinetics of copper sulfidation, discussed below, and the measured grain morphology of the Cu_2S grains at high RH, discussed in section 5.

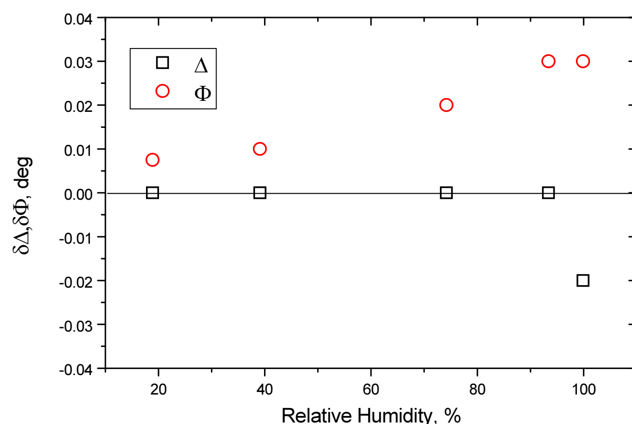

Fig. 4. Ellipsometry-determined parameters, Δ and Φ, for Cu_2O as a function of RH. Δ reflects changes in thickness and Φ reflects changes in refractive index. The primary effect of increasing RH is to increase the refractive index (polarizability) of the film.

3.2. Nucleation

In order to understand the nucleation of Cu_2S (i.e. the initial stages of sulfidation), the morphology, uniformity, and density of the Cu_2S film was studied using x-ray reflectivity (XRR), scanning electron microscopy (SEM), and atomic force microscopy (AFM). Cu samples were prepared by evaporation of Cu metal on to Si wafers and were then sulfidized. For these experiments, the reactor designed permitted optical access to the sample during sulfidation, and optical endpoint detection using a system developed by Bill Breiland (Org. 5526) [18] was used to interrupt the sulfidation process after a predetermined extent of reaction, see Fig. 5.

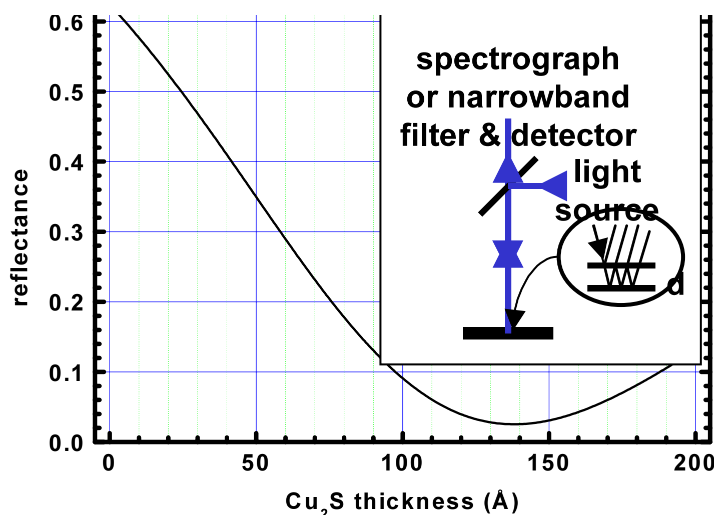

Fig. 5. The optical reflectance signal obtained during the sulfidation of Cu. For studies of nucleation, the sulfidation was interrupted at a relative reflectance of 0.5 or 0.3, corresponding to a sulfide thickness of approximately 25 to 50 Å.

Following the short sulfidation times, the presence of Cu_2S was measured by energy dispersive analysis by x-rays (EDAX). Differences were observed between sulfidation at high

and low RH. At high RH, a clear sulfur signal is present in the EDAX signal when the sulfidation is stopped following a drop in reflectance to 0.5 of the initial value. For sulfidation at low RH, no clear sulfur is detected until the optical reflectance drops to 0.3, nominally indicating a sulfide thickness twice that of the high RH growth.

SEM and AFM showed that the thin nucleated sulfide layer is morphologically different at low and high RH, see Fig. 6. At high RH, the Cu_2S nuclei are distributed non-uniformly (i.e. patchy in appearance), exhibiting thickness variations on a lateral length scale of about 10 μm. At low RH, the sulfide nuclei are uniformly distributed, forming a Cu_2S layer of approximately constant thickness. As will be discussed in section 5, these differences in the Cu_2S morphology, viz. the nodular appearance of the sulfide at high RH and the more uniform sulfide at low RH, are carried through into the bulk sulfide that forms following long term sulfidation.

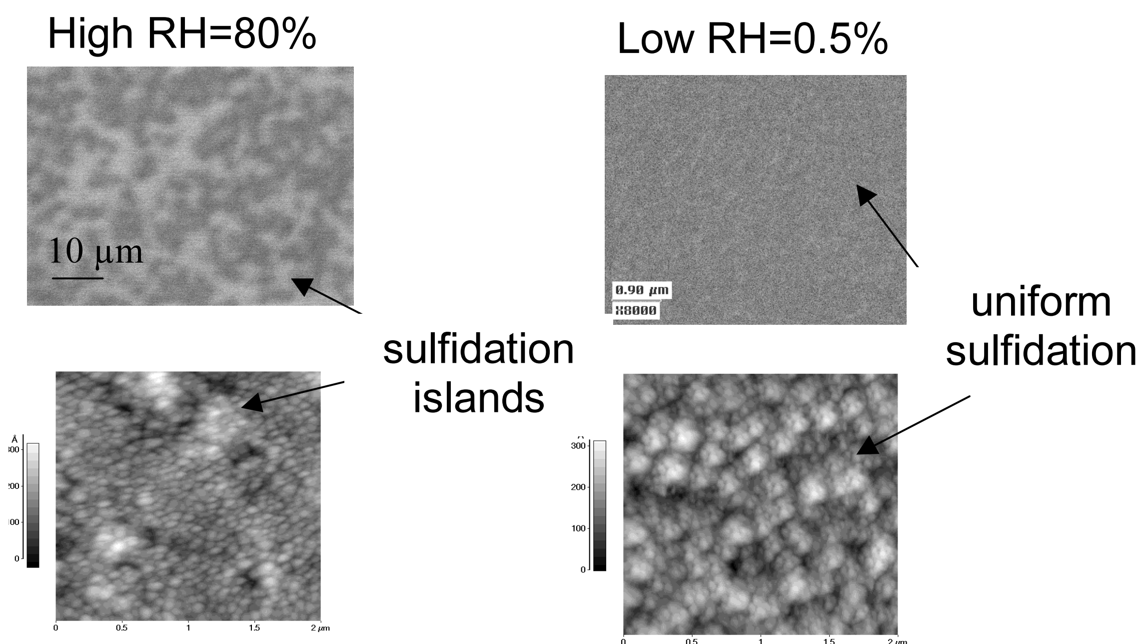

Fig. 6. SEM (top) and AFM (bottom) of the initial stages of Cu sulfidation at high and low RH. Sulfidation at high RH is initially patchy with nodular sulfide nuclei, while sulfidation at low RH is more uniform.

In addition to the SEM/AFM studies, XRR reveals that the Cu_2S formed at low RH can be modeled as a uniform film with a density of 5.6 g/cm^3 (the bulk density for Cu_2S in the chalcocite phase), while the film that was formed at high RH requires modeling as at least a two layer film with a film density near the interface of 5.6 g/ cm^3 and a density near the surface of 4.5 g/ cm^3. This is suggestive of higher porosity in the Cu_2S formed at high RH, which is confirmed by transmission electron microscopy, discussed in section 5.2.

3.3. Stage I Kinetics

The kinetics of stage I sulfidation (the initial linear part shown in Fig. 2), was evaluated through temperature-dependent studies of sulfidation at low and high RH. The kinetics in stage I is expected to be thermally activated, i.e.

$$\text{Cu}_2\text{S thickness} \propto k't \exp(-E_A/k_BT), \quad (3)$$

where k' is a reaction rate constant, t is time, and E_A is the activation energy for the process. From measurements of the sulfidation rate in the linear stage I regime as a function of temperature, an Arrhenius plot is obtained, see Fig. 7, from which the activation energy for the stage I reaction can be obtained.

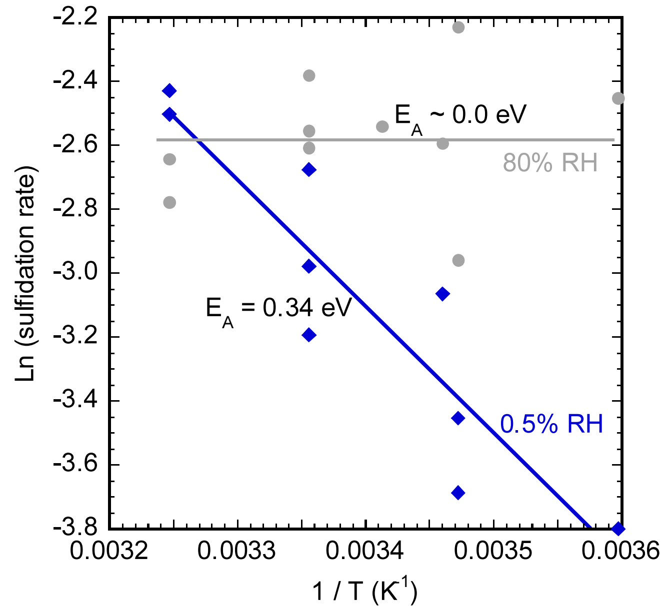

Fig. 7. Arrhenius plot to determine the activation energy for the rate limiting reactions in stage I sulfidation of Cu at low and high RH. Very different activation energies are seen for low and high RH sulfidation.

As shown in Fig. 7, an activation energy of 0.34 eV is obtained for the stage I process for low RH sulfidation, while the activation energy is close to zero for sulfidation at high RH. This indicates that the sulfidation at low and high RH fundamentally follows a different process, at least during the initial stages. The value of the activation energy for sulfidation at low RH is consistent with a generic class of surface reactions, e.g. $H_2S_{(adsorbed)} \rightarrow H_{(adsorbed)} + HS_{(adsorbed)}$. Exactly which surface reaction is rate-limiting is not clear, however. The low value for the activation energy for stage I sulfidation at high RH suggests that the stage I sulfidation is not rate-limited by a simple surface reaction. Instead, based on this data, and other data not shown, it is suggested that sulfidation at high RH is controlled by other processes with low activation energy, such as gas phase mass transport of $H_2S_{(g)}$ or liquid phase mass transport of a particular speciation product. The observation that the initial sulfidation rate near room temperature is similar at low and high RH (see Fig. 2), is mere coincidence – there is nothing in the kinetic data to suggest that the initial sulfidation is controlled by the same set of reactions for low and high RH sulfidation, and this likely has a profound effect on the resulting morphology of the Cu_2S layer that is observed and is discussed in section 5.

4.0 Micro-patterned Test Structures for Sulfidation

An important aspect of this project was the development of novel micro-test structures that offer promise to shed insight into Cu sulfidation mechanisms. Several test structures were developed and preliminary information was obtained to assess their utility for sulfidation studies.

4.1. Background

The micro-test structures developed in this project were based on a set of micro-test structures that were previously developed by us at Sandia for use in enabling electrical or optical monitoring of atmospheric corrosion [18]. Some of these older structures, along with the new structures developed for this project, are shown in Fig. 8. As shown in Fig. 8, the total size of the structures was chosen to permit easily-handled samples of 1 to 2 cm in dimension. In all cases, the structures were created using conventional photolithographic patterning applied to thin films of Cu atop SiO_2-coated Si or to bulk polycrystalline Cu disks. Photolithographic patterning permitted the creation of micro-test structures with critical dimensions less than 5 μm.

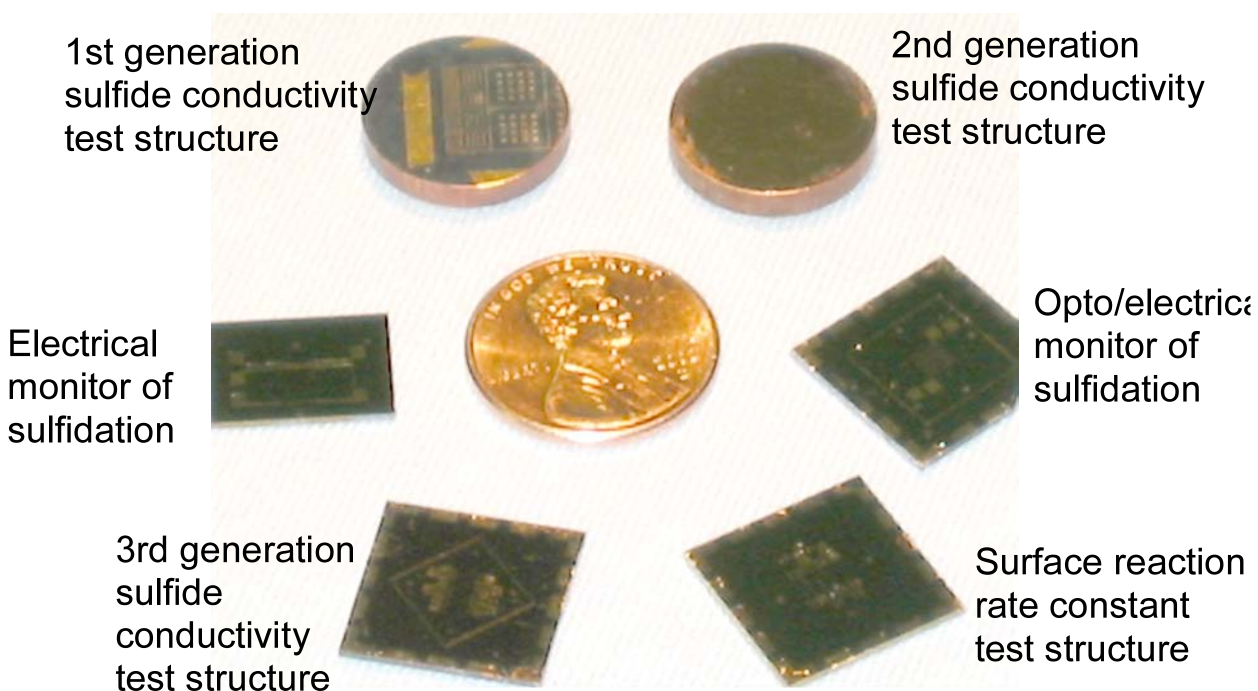

Fig. 8. Picture of several micro-test structures developed for atmospheric corrosion studies. Two of the test structures (the electrical monitor of sulfidation and opto/electrical monitor of sulfidation) were developed prior to this LDRD project.

The prior test structures were based on meander line structures designed as electrical resistance test structures or as optical gratings. Figure 9 describes the electrical test for Cu sulfidation. The structure consists of three separate Cu meander lines with Cu line width = 20 μm. Two of the lines are interdigitated, and a third line is separated from the others to act as a control. Processing is performed in the region of the interdigitated lines to affect the Cu sulfidation rate. The extent of Cu sulfidation is monitored *in situ* by measuring the increase in

Cu line resistance due to the conversion of highly conductive Cu to the much lower conductivity Cu_2S. Using these types of structures, it was determined that indium and aluminum impurities reduce the sulfidation rate while hydrogen impurities (implanted as the isotope deuterium) accelerates the sulfidation rate [14,18]. Some of these effects can be understood on the basis of vacancy complexation in the sulfide.

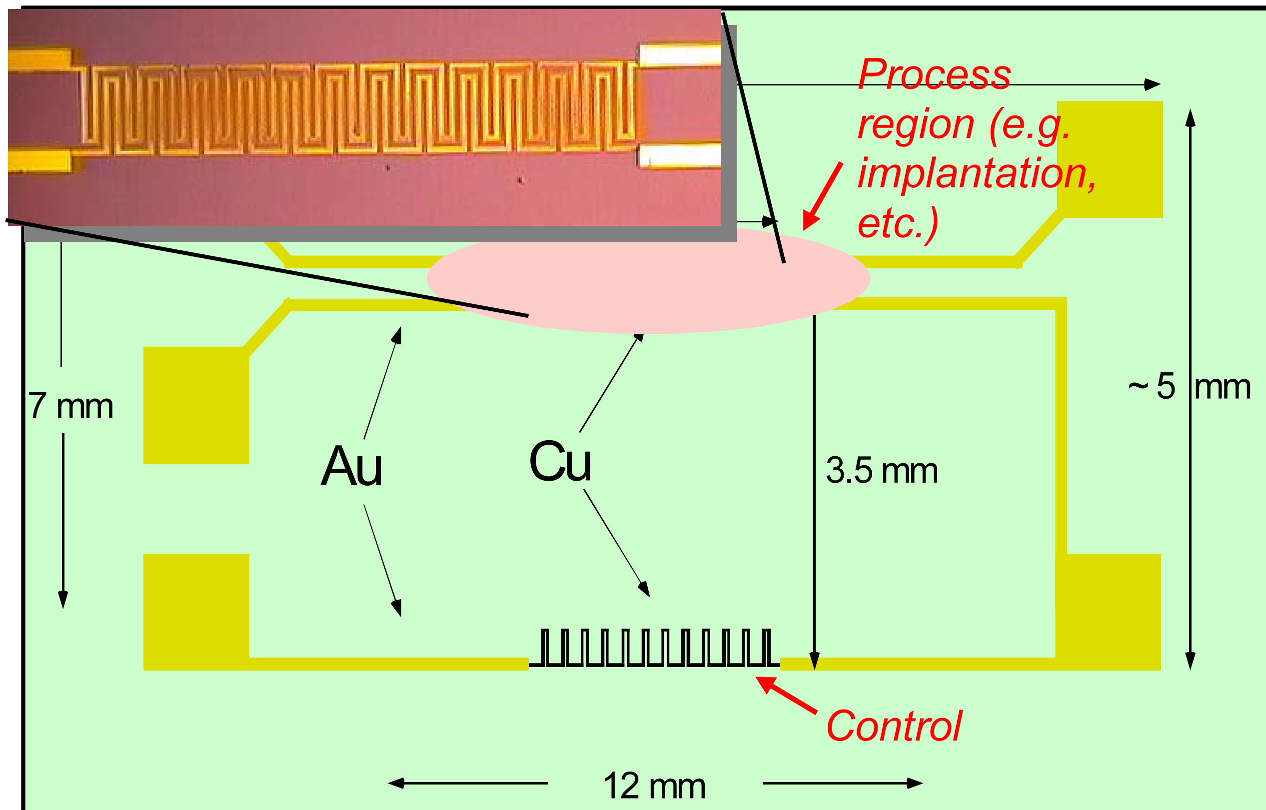

Fig. 9. An electrical monitor of Cu sulfidation designed for in situ monitoring of the extent of Cu sulfidation. The electrical resistance of the Cu meander line is measured, which is observed to increase as sulfidation progresses. The inset is a close-up picture of the actual device.

Another test structure is shown in Figure 10. This structure is designed to act as an optical grating. The principle is similar to the electrical test structure, but in this case sulfidation leads to a physical change in the width of the Cu lines, which start out as 20 µm in width and are spaced by 20 µm. During sulfidation, optical diffraction from the grating is measured, and the shift in the diffraction spot is used an indicator of the extent of Cu sulfidation. The structure is also designed for *in situ* electrical detection of sulfidation by measurement of the change in resistance of the single large Cu meander line.

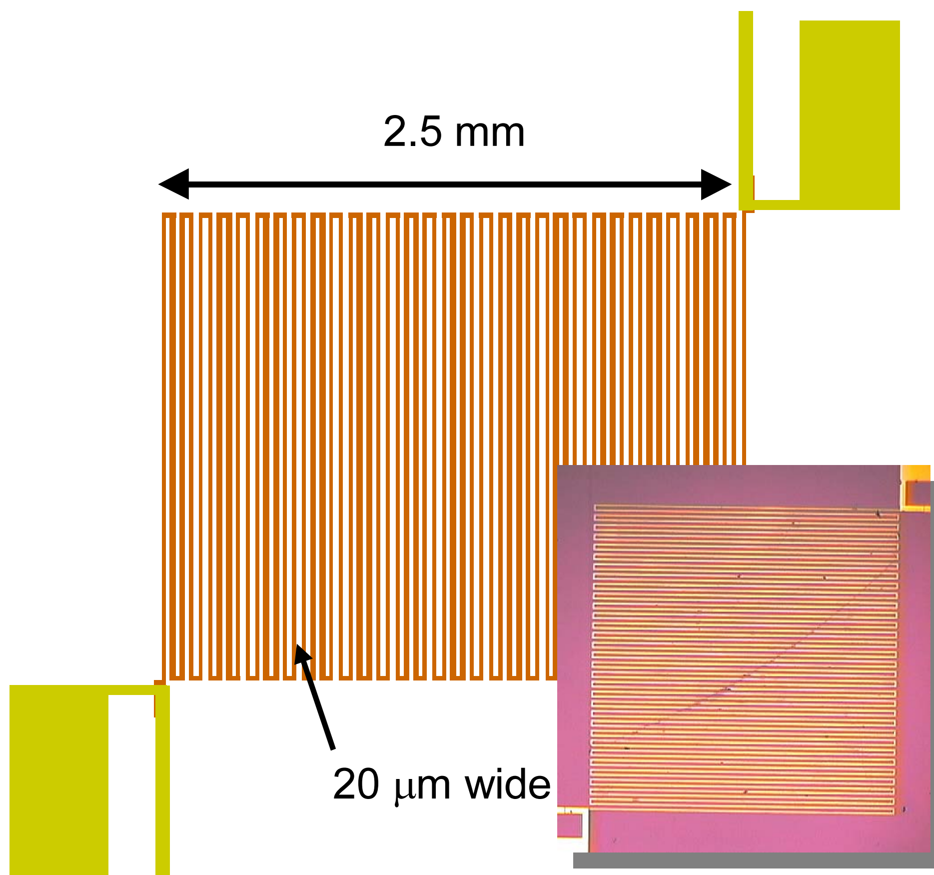

Fig. 10. An optical monitor of Cu sulfidation based on a diffraction grating consisting of a Cu meander line of 20 μm width and 20 μm spacing. The inset is a picture of the actual device.

4.2. Micro-loading Test Structures

In this project, the focus is on how RH influences the sulfidation behavior of Cu. As was shown in section 3.3, the kinetics of the initial stages of sulfidation is very different at low and high RH. In an effort to understand the rate-limiting processes that control the sulfidation of Cu, a micro-test structure was developed to look at the rate of the surface reaction, k. It is difficult to measure the surface reaction rate directly. However, due to an effect known as micro-loading, the surface reaction rate can be measured relative to the rate of gas phase diffusion, D [18]. Micro-loading is a phenomenon that occurs in certain gas phase reactions which are reactant-limited. The effect is characterized by the depletion of the reactant species, H_2S in this case, from the gas phase leading to a starved chemical reaction at the surface. If the reactant gas is passed over a large surface, the surface on the leading edge of the gas flow will scavenge the reactant from the gas flow, leading to an increased extent of reaction in this region compared to the region downstream from this site. For similar reasons, physically small structures will experience an average greater amount of reaction than larger structures. For a continuously stirred reaction vessel or a reaction vessel that produces a uniform reactant concentration impinging on the sample, a characteristic reaction profile is expected depending on the size of the sample. In the case of a sample that consists of long, narrow lines, the extent of reaction (sulfide thickness in our case), is expected to be larger at the edges of the lines than at the center of the line. If the rate of supply of the reactant in the gas phase (D) is large compared to the rate at which the reactant is consumed at the surface (k), then the effect of micro-loading (i.e. the

thickness at the edge of the sample compared to the thickness in the center) is expected to be small, and vice versa.

To measure the micro-loading effect and, hence, the ratio D/k, a micro-test structure was developed that consists of an array of Cu lines of widths varying from 5 μm to 100 μm, see Fig. 11. This structure was formed by patterning photoresist on an SiO_2-coated Si wafer, followed by Cu deposition using evaporation under high vacuum conditions, and then lift-off (a patterning step in which the Cu is patterned by removing the Cu lying atop the photoresist-covered regions of the sample – this is achieved by dissolving the photoresist in a solvent). Following creation of the micro-loading samples, the samples were sulfidized at low RH and high RH in $H_2S_{(g)}$ concentrations of 160 ppb. Following sulfidation, the Cu lines on the samples were cross-sectioned using focused-ion-beam (FIB) etching, and the etched surfaces were examined by SEM. Fig. 12 shows FIB cross sections of two representative lines on a sample that were sulfidized at 80% RH, one 5 μm wide line and a different 100 μm wide line.

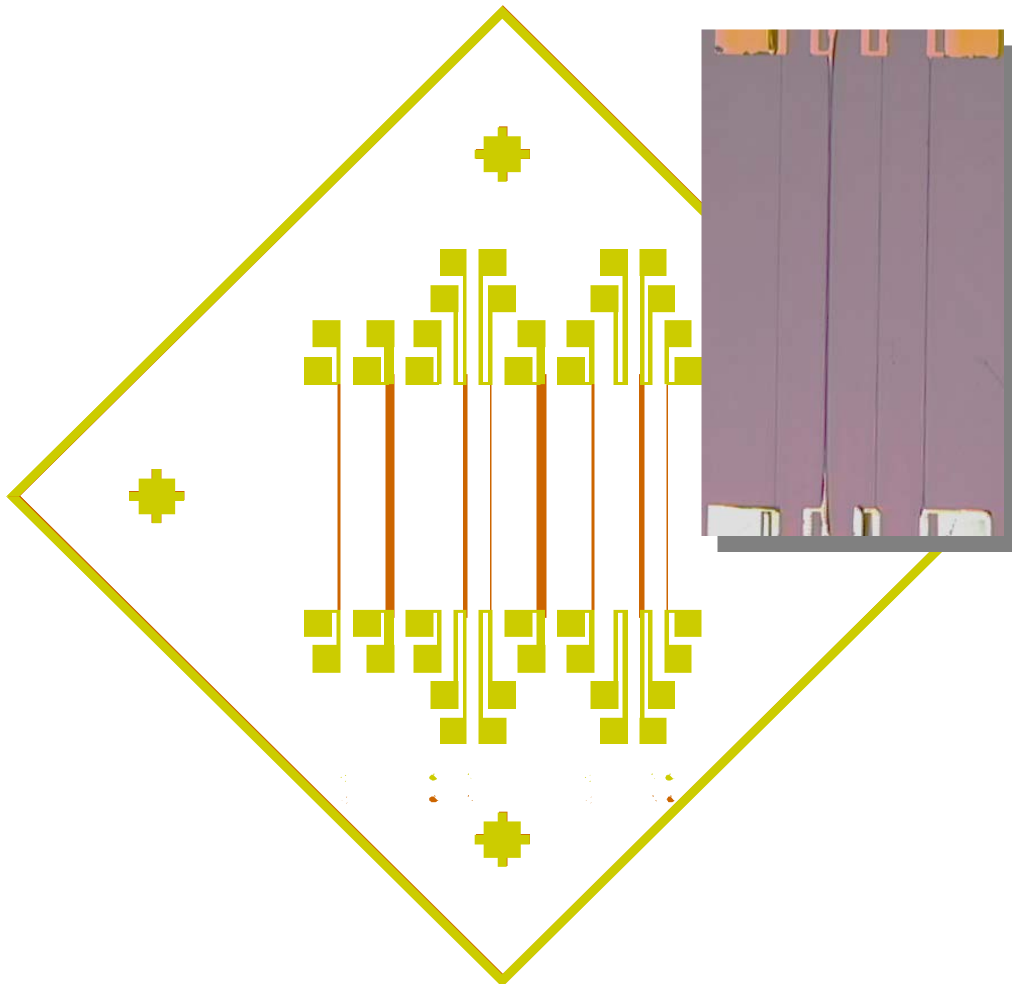

Fig. 11. The micro-loading test structure. The sample consists of patterned Cu lines of widths ranging from 5 μm to 100 μm and lengths approaching 5 mm. Au contacts were also patterned on the ends of the lines to permit in situ monitoring of Cu sulfidation using the measurement of resistance changes. The inset is a close-up picture of one of the actual devices.

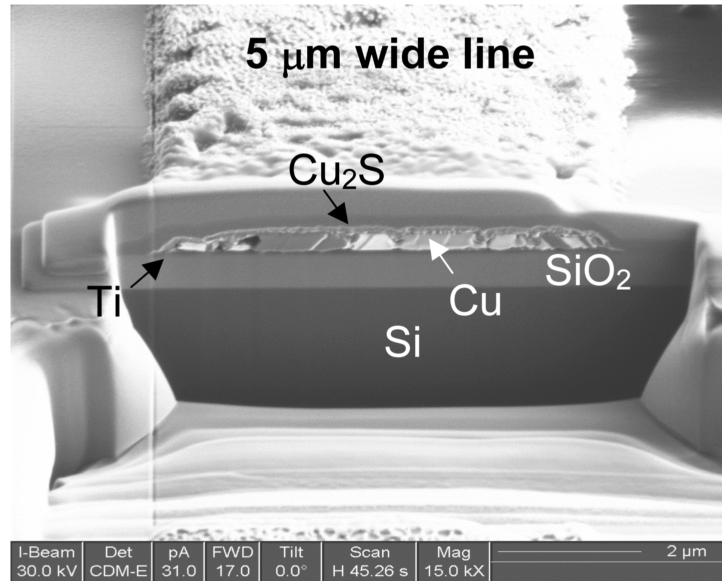

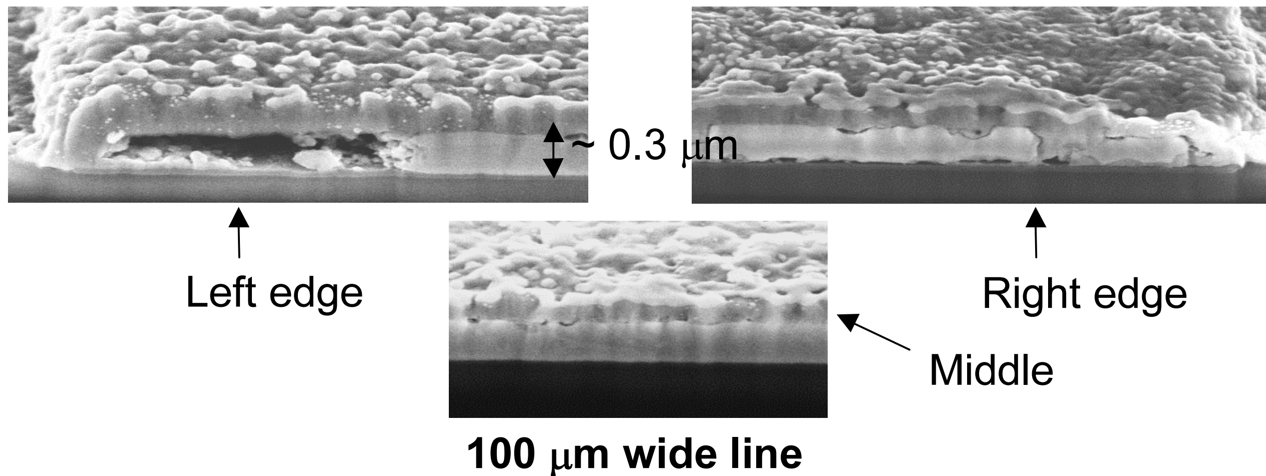

Fig. 12. FIB cross-sections of 5 μm and 100 μm wide Cu lines following sulfidation at 80% RH. Micro-loading results in an increased thickness at the edges of the lines compared to the center.

Based on the measured sulfide thicknesses at the edges and center of the 100 μm line, an estimate of D/k can be made, see Fig. 13. The ratio of edge to center thickness suggests a D/k value that is less than 100 but much greater than 10. (A more accurate analysis would require the examination of a greater number of sulfidized Cu lines.) The ratio of D/k at *low* RH was not obtained, however, due to the unexpectedly light sulfidation of the Cu lines at 0.5% RH (the sulfide thickness based on FIB cross-sections was < 20 nm – too thin to permit an accurate measurement of sulfide thickness). The value of D/k obtained from the micro-loading experiment is in the correct range of D/k values that was obtained by fitting simulations of Cu sulfidation to experimentally-measured sulfidation rates [18,19]. The conclusion from this is that it should be possible to enter regimes in which the sulfidation rate is controlled by the rate of the surface reaction, not by gas phase diffusion, and this is likely to be the case for sulfidation at low RH.

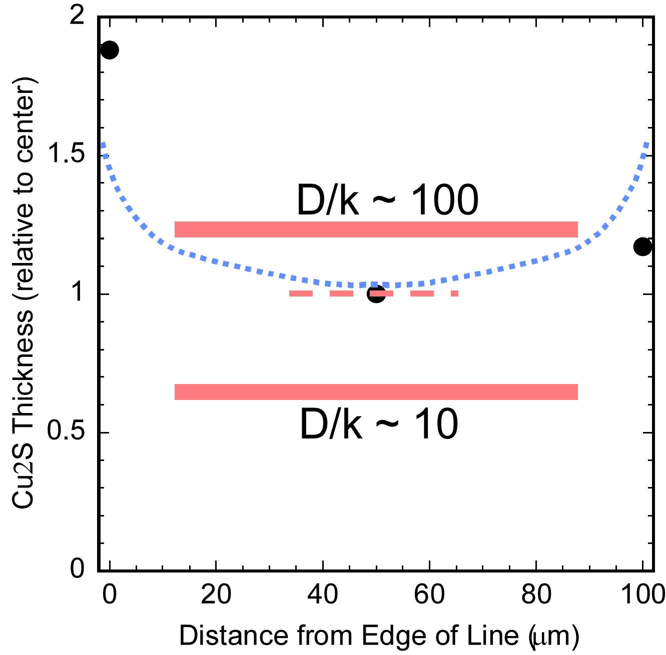

Fig. 13. Cu_2S thickness as a function of distance from the edge of a 100 μm wide Cu line that was sulfidized at 80% RH. The red lines correspond to the expected thickness at the center of the line if D/k were 10 or 100. The experimental result indicates that D/k is >> 10 but < 100.

4.3. Electrical Conductivity Test Structures

One of the challenges of characterizing materials is measuring and characterizing point defects, such as vacancies, interstitials, etc., that might be present. In general, point defects are not measurable by direct means, such as high resolution TEM (HRTEM), so typically some spectroscopic measurement is required. In the case of Cu sulfide, there is a unique opportunity to measure point defect concentrations through the use of electrical conductivity measurements. In order to perform these measurements, electrical conductivity micro-test structures were developed.

Electrical conductivity measurements should enable the measurement of vacancy concentrations in the Cu_2S, which, in turn, is important for controlling the solid state diffusivity of Cu through Cu_2S. This can be understood as follows: Cu_2S is a p-type semiconductor with band gap equal to 1.8 to 2 eV [20]. Cu vacancies in Cu_2S, V_{Cu}', act as an acceptor, creating a hole in the valence band, i.e. $Null \rightarrow V_{Cu}' + h^{\bullet}$. For an extrinsic semiconductor like Cu_2S, the electrical conductivity, σ, is proportional to the hole concentration, which equals the Cu vacancy concentration, i.e.

$$\sigma = [h^{\bullet}]e\mu_h = [V_{Cu}'] e\mu_h, \qquad (4)$$

where *[]* is the concentration of the species in the bracket, *e* is the electronic charge, and $e\mu_h$ is the hole mobility. For vacancy-mediated diffusion, the diffusion constant, D_{Cu} is proportional to

the vacancy concentration, i.e. $D_{Cu} \propto [V_{Cu}']$. Therefore the Cu diffusivity should also be proportional to the electrical conductivity of the film, i.e. $D_{Cu} \propto \sigma$, and a measurement of the electrical conductivity should enable estimation of the Cu diffusivity in the bulk Cu_2S grains. An important point needs be made regarding this analysis: While this analysis may be valid for bulk diffusion *within* the Cu_2S grains, if the diffusivity through the Cu_2S film is limited not by bulk diffusion but by diffusion along grains or across grain boundaries, then the direct correlation of electrical conductivity with observed Cu diffusivity across a Cu_2S film is not expected to be valid. As we will show in section 5, there is indeed evidence that Cu diffusivity is not limited by bulk diffusion within the Cu_2S grains, at least for Cu_2S formed at high RH.

The simplest micro-test structure that was developed to measure electrical conductivity in Cu_2S is shown in Fig. 14. The structure consists of arrays of patterned Au contacts ranging in size from 50 μm square up to 400 μm square. For these structures, patterning was performed on bulk poly-crystalline Cu coupons, demonstrating the feasibility of patterning samples of non-ideal geometry, i.e. non-Si-wafer-based samples. The electrical conductivity of the Cu_2S was measured using two point measurements, which is a non-ideal measurement. As is shown in Fig. 15, an approximate electrical conductivity of Cu_2S that was formed at high RH, was found to be less than 3×10^{-4} $ohm^{-1}cm^{-1}$. However, it is clear that there is current spreading affecting the measurement, as evidenced by the increase in apparent conductivity for the smallest contact sizes (an edge effect). More accurate measurements require the sulfidized region to be physically defined by an aperture and the use of 4 point contact measurements. Micro-test structures incorporating these improvements were also developed.

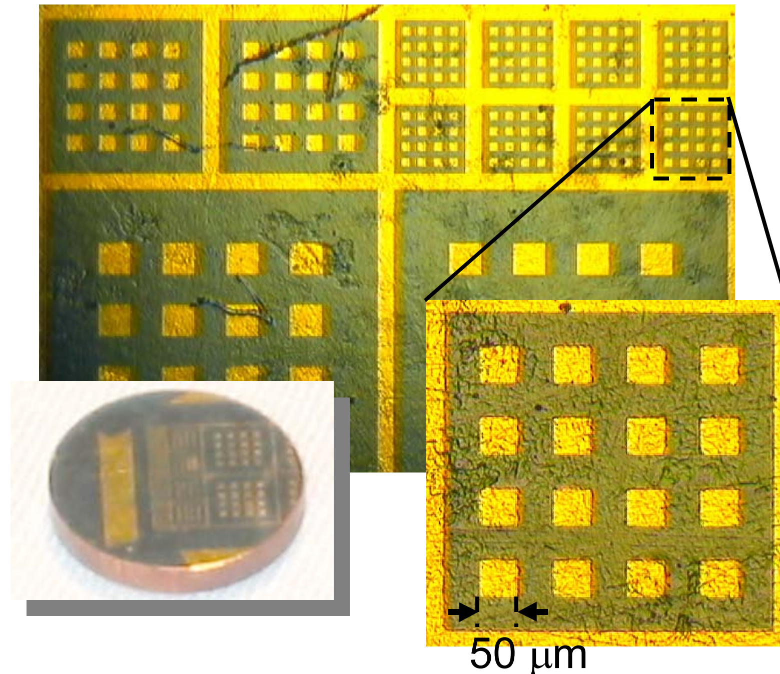

Fig. 14. One design for a simple electrical micro-test structure. In this design, Au contacts of dimensions ranging from 50 μm × 50 μm up to 400 μm × 400 μm were lithographically-defined on to a sulfidized bulk polycrystalline Cu coupon.

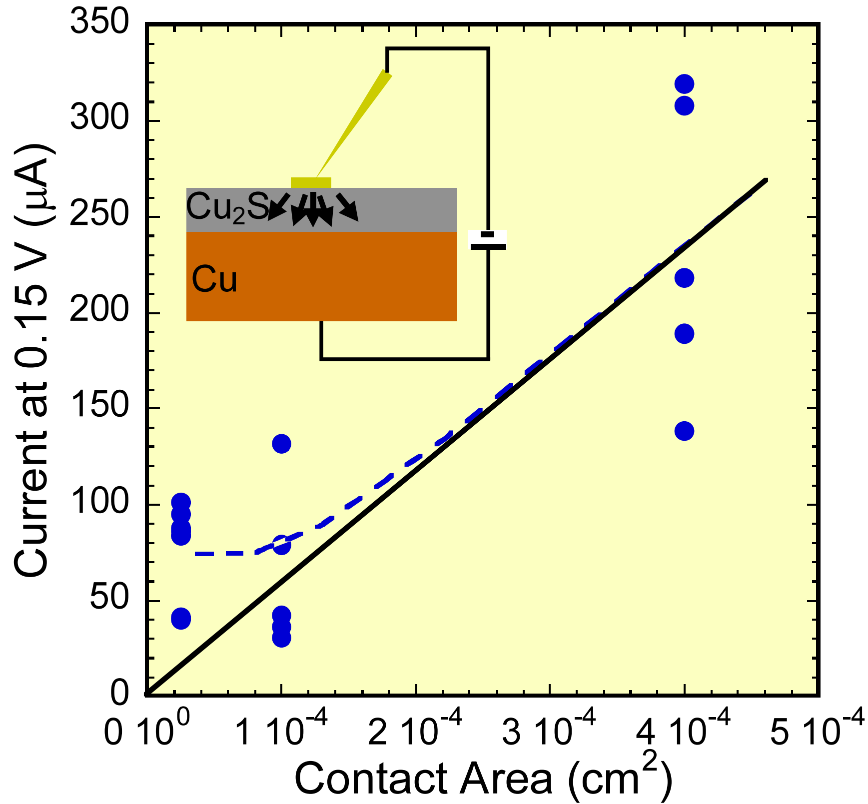

Fig. 15. The measured current at 0.15 V as a function of contact area for a bulk Cu coupon that was sulfidized at 80% RH to a thickness exceeding 1 μm. The inset shows the measurement geometry and the problem of spreading resistance that creates measurement inaccuracy for small contact areas.

Figure 16 shows the design of the of the improved electrical mico-test structure, and Figure 17 shows the process flow. The structure is more elaborate, using three mask levels and two alignment steps. The first step involves patterning the Cu layer to create a series of structures that have two electrical connections to a central region. The subsequent step involves the deposition and patterning of an inert insulating layer that acts as an aperture to confine the sulfidation into regions ranging in size from 5 μm × 5 μm up to 100 μm × 100 μm. The sample is then sulfidized. After sulfidation, Au contacts are patterned over the Cu region to enable electrical contact to the top Cu_2S layer and the Cu layer beneath. Four contacts are made to zero out the lead resistance.

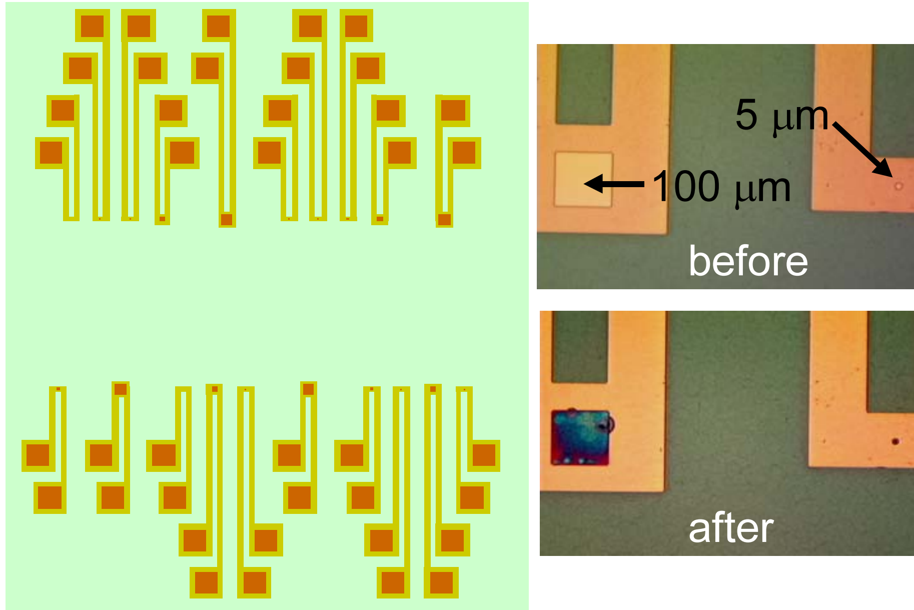

Fig. 16. The improved electrical micro-test structure. The pictures on the right show a close-up of some of the actual test structures before and after sulfidation.

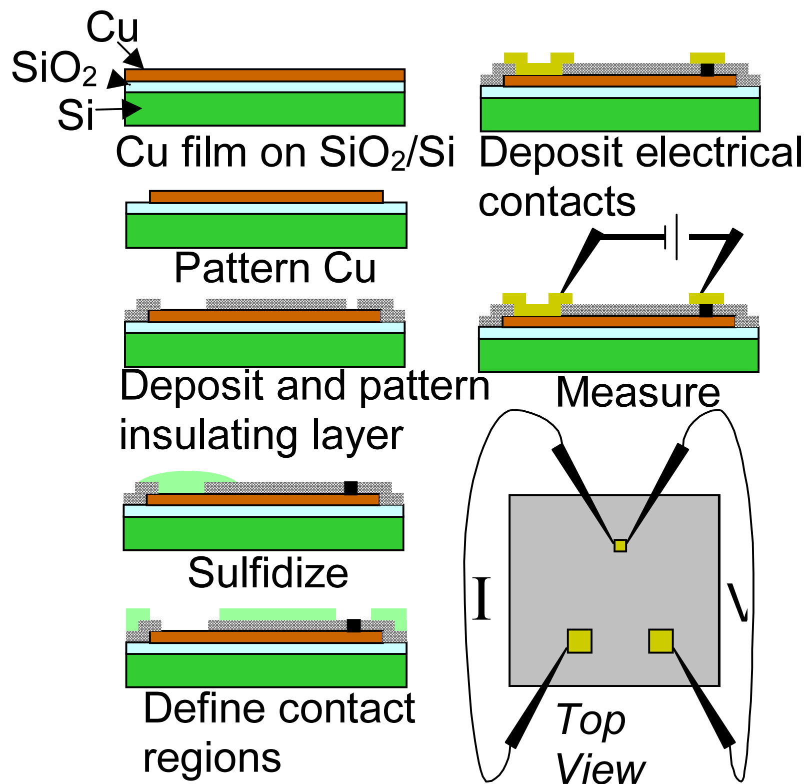

Fig. 17. The process flow for the improved electrical micro-test structure. The structure requires three patterning steps (3 mask levels), but creates well-defined sulfidized regions and permits 4-point electrical contacts.

The structures shown in Fig. 16 were fabricated and tested. Problems were found, however, in the deposited and patterned insulating layer. N-parylene was used as the insulator, which is desirable for its insulating and inert characteristics. Parylene was not found to be stable however in the final processing steps to create the structure (the lithographic patterning of the Au contacts). It was found that the parylene developed cracks at some point during the photoresist deposition, 90°C curing, UV exposure, and developing. This allowed the evaporated Au contacts to contact un-sulfidized Cu, shorting out the Cu_2S layer. Since that time, more recent processing improvements have been developed, the most important being a hard baked SU-8 insulating layer. This chemistry shows greater promise for the development of the structures shown and described in Figs. 16 and 17, but new electrical micro-test structures have yet to be fabricated.

In summary, the new micro-test structures described in this section resulted in new experimental knowledge of the relative rate of the surface sulfidation reaction and offered the possibility for measurement of the vacancy concentration of Cu_2S and correlation of this vacancy concentration with the solid state diffusivity of Cu through Cu_2S. However, it was subsequently discovered that Cu diffusivity through Cu_2S that was formed at high RH may not be controlled by bulk diffusivity through the Cu_2S grains (this is discussed in section 5). This raises doubts on the utility of electrical test structures for answering the mystery of the different sulfidation rates at low and high RH. However, the electrical test structures are still useful for characterizing the electrical conductivity of Cu_2S as a function of environmental variables during growth, and this is important information for the modeling of the aging of Au-coated Cu connectors.

5.0 Microstructural Characterization of Copper Sulfide

Microstructural studies were performed to identify the phase, surface topography/morphology, and grain morphology for copper sulfide layers formed on Cu at low and high RH. The morphological studies, particularly the grain morphologies at high and low RH were particularly useful for identifying possible sulfidation mechanisms. These studies are discussed in the following sections.

5.1. Phase Identification of Copper Sulfide

To determine whether sulfidation at low and high RH produces a different structure of Cu_2S, the crystal structure of the Cu_2S corrosion product formed at low and high RH was examined by x-ray diffraction (XRD) and selected area electron diffraction. The XRD results are shown in Fig. 18. For both low and high RH exposure during sulfidation, copper and sulfur react to form the low chalcocite phase (Cu_2S). This identification was also confirmed locally on the samples using selected area electron diffraction in a TEM. The XRD results indicate significant differences in texturing (grain orientation) between the sample sulfidized at 0.5% RH and the sample sulfidized at 80% RH. For the low RH samples, we see dominant reflections at d=3.28 Å, d=2.21 Å and d=1.88 Å, corresponding to orientations of ($\bar{3}04$) + ($\bar{1}04$), ($\bar{3}16$), and ($\bar{5}36$) + ($\bar{1}36$) + ($\bar{7}06$) + (106), respectively. For the high RH samples, we see dominant reflections at d=2.76 Å and d=1.99 Å, corresponding to orientations of (630) and (240), respectively. This indicates that there is a microstructural difference between the sulfide grown at low and high RH and suggests the use of TEM analysis.

The low chalcocite phase (Cu_2S) is monoclinic (P21/c space group), with a unit cell volume of 2191.5 Å^3, 144 atoms in the unit cell, and a density of 5.5-5.7 g/cm^3 [21]. Theoretical calculations of diffusion in this low chalcocite system have been performed by A.Wright (Sandia, Org. 1112) [22], and it was found that copper vacancies diffuse readily through Cu_2S. This is not surprising considering the open crystal structure is pretty open and the many unoccupied and partially occupied copper sites that would provide pathways for diffusion, see Fig. 19. Furthermore, the structure also exhibits pseudo-hexagonal sheets of S atoms, providing an almost layered-like structure for the Cu_2S, see Fig. 19.

The result of the phase identification study is that the same phase of Cu_2S forms whether sulfidation occurs at high or low RH, so differences in sulfidation rates are not due to differences in the sulfide phase that forms.

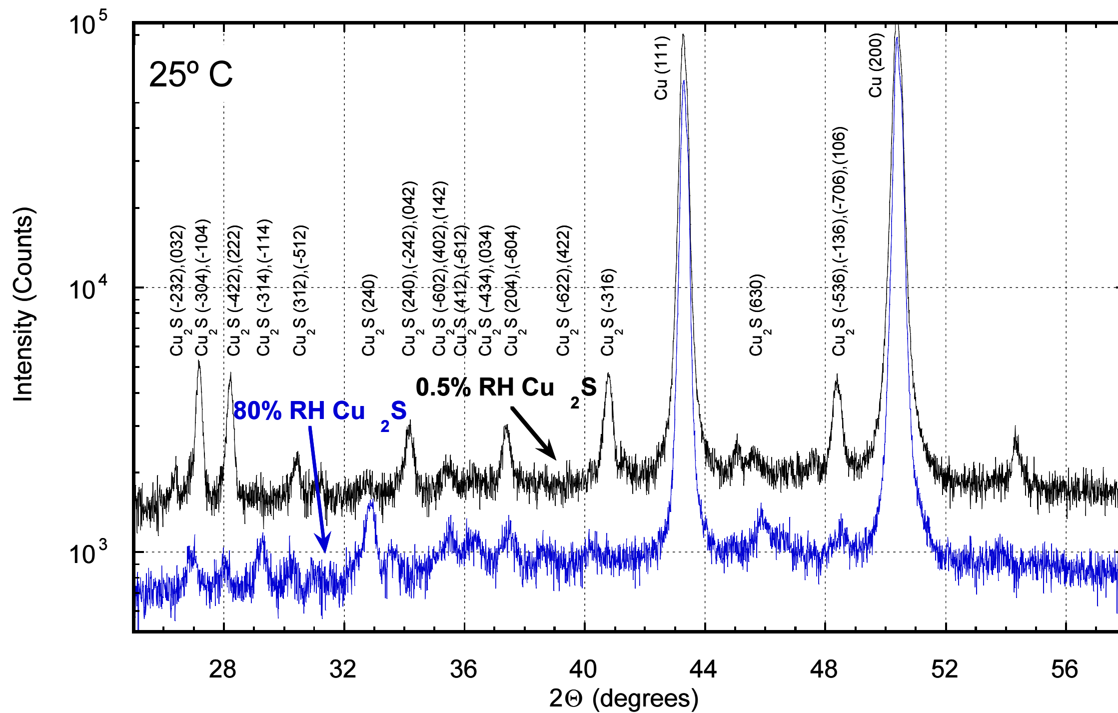

Fig. 18. X-ray diffraction from two Cu_2S films, one formed at high RH and the other formed at low RH. In both cases, the chalcocite phase of Cu_2S is observed, although the texturing of the film (i.e. the dominant reflections) is different at low and high RH.

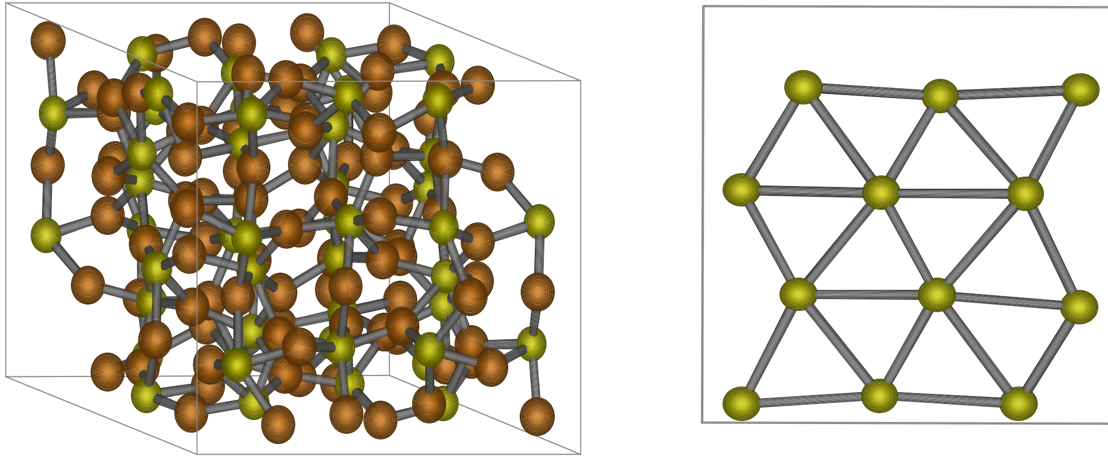

Fig. 19. Schematic view of the crystallographic structure of Cu_2S. Copper colored spheres represent sites occupied by Cu atoms and yellow colored spheres represent sites occupied by S atoms. Right: schematic view of the pseudo-hexagonal sheets of S atoms present in Cu_2S.

5.2. SEM Surface Characterization

The surface morphology of the Cu_2S layer formed at low and high RH was examined by scanning electron microscopy (SEM). For sulfidation performed at a temperature of 15°C, there are noticeable differences in surface morphology for Cu_2S layers formed at high and low RH, see Fig. 20. However, for sulfidation performed at room temperature and above, e.g. 25°C to 35°C, there are not clear discernible differences detected in the sulfide by SEM, see Fig. 21. The surface of the sulfide at high RH exhibits a slightly rougher surface and roughness on a larger length scale, but part of the reason for these differences could be due to the greater film thickness for the high RH grown samples. The conclusion from SEM studies is that there are no clear discernible features in surface morphology at low and high RH to explain the observed differences in sulfidation rate. This suggests the need for the more detailed structural studies afforded by transmission electron microscopy (TEM) and discussed below.

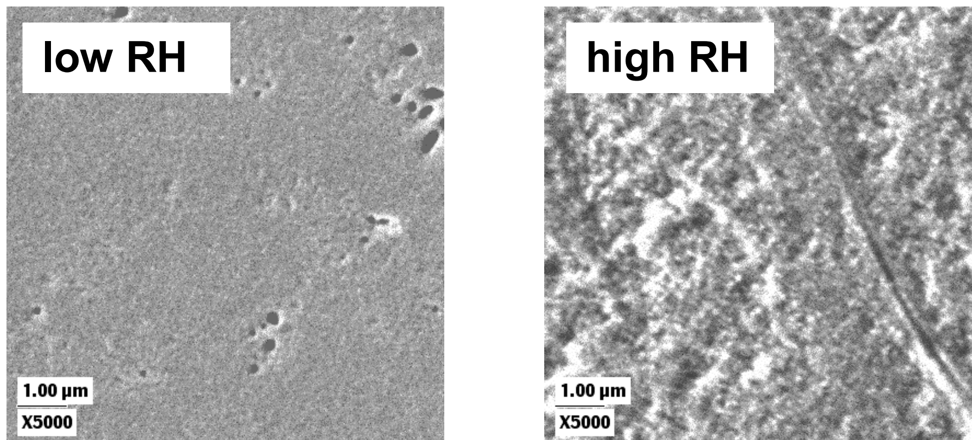

Fig. 20. Comparison of the SEM surface morphology for Cu_2S films formed at low and high RH at 15°C. A rougher surface is seen for high RH sulfidation.

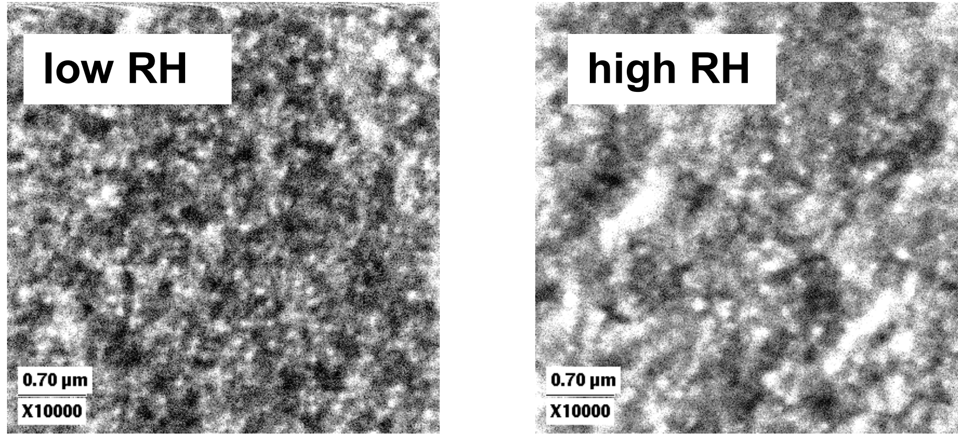

Fig. 21. Comparison of the SEM surface morphology for Cu_2S films formed at low and high RH at 25 ℃ and 35 ℃. In this temperature range, no clear surface morphological differences are seen between low and high RH sulfidation.

5.3. TEM Microstructure Characterization

TEM and high resolution TEM (HRTEM) were performed on samples sulfidized at low and high RH in order to look for microstructural clues to the differences in observed sulfidation rates [23-25]. Figure 22 shows four cross-section TEM micrographs, two for low RH and two for high RH. The upper two micrographs are from samples that were sulfidized to a nominal thickness of about 100 nm, while the lower two micrographs are from a low RH sample with a Cu_2S layer about 400 nm thick and a high RH sample with a Cu_2S layer about 200 nm thick. For each sample, representative grains are highlighted (dark field imaging, not shown, was used to identify the position and extent of the grains, especially for the lower magnification images). The average grain size for the films sulfidized at high RH is small, about 20 – 50 nm in size, and independent of film thickness. In contrast, the grains for the films sulfidized at low RH are larger and typically span the entire film thickness, suggesting that the Cu_2S grains grow continuously during the sulfidation process, i.e. solid phase epitaxy on to existing grains.

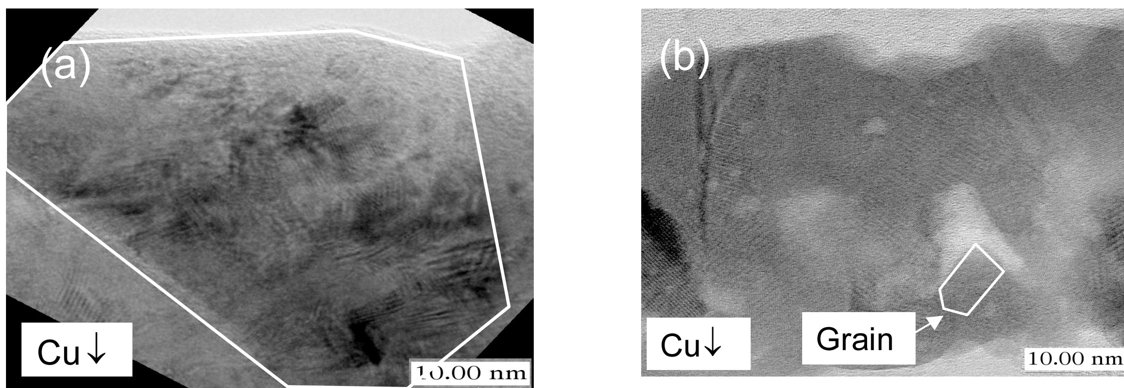

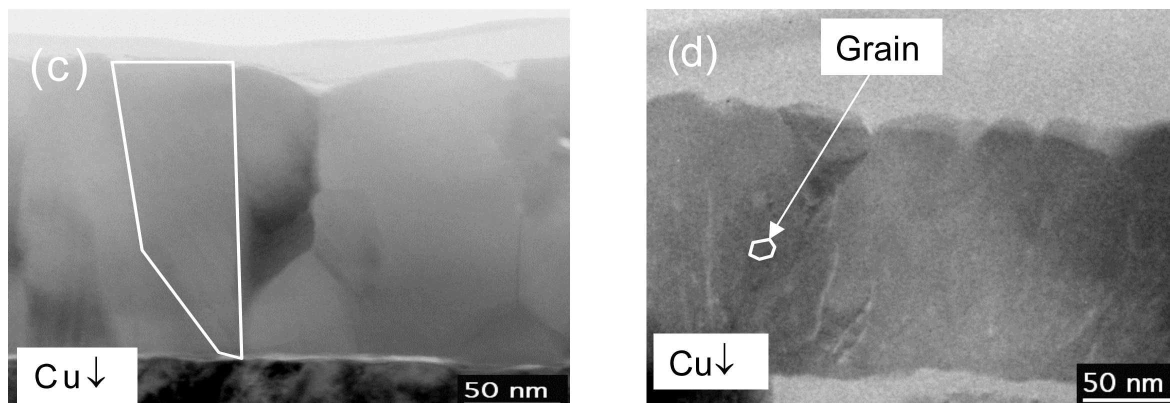

Fig. 22. Bright-field TEM and HRTEM images of Cu_2S films formed at low and high RH at 25 ℃. (a) low RH, 100 nm thick, (b) high RH, 100 nm thick, (c) low RH, 400 nm thick, and (d) high RH, 200 nm thick. The white boxes outline representative grains.

The light-colored lines that run vertically in Fig. 22(d) and that appear to delineate columnar grains are actually regions of low density, which are consistent with voids. These are discussed in more detail below. The actual grains are much smaller, as shown in the outlined region. Taking a closer look at the microstructure, Fig. 22(c) shows preferential grain orientations and grain-boundary grooving, both of which are consistent with significant grain growth. HRTEM imaging of the grain boundaries for the low and high RH samples are shown in Fig. 23. The grain boundaries in the low RH samples are clean and abrupt. In contrast, the high RH samples have poorly connected and voided grain boundaries and no preferential grain orientations. The low density regions, or porosity, is also readily visible in the high RH samples. These low density regions are apparent in high concentration for all of the high RH samples examined, but they are absent in the low RH samples.

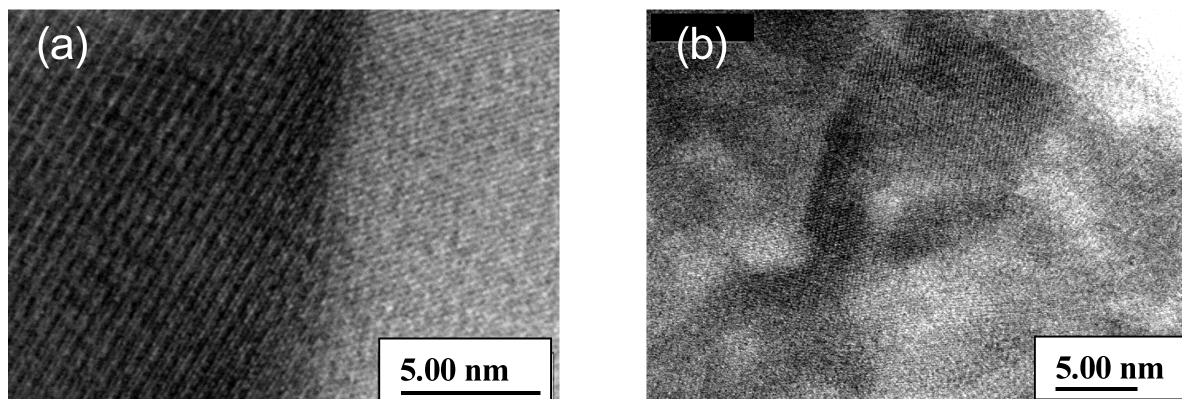

Fig. 23. HRTEM images of grain boundaries in (a) a Cu_2S film formed at low RH, and (b) a Cu_2S filmed at high RH. The HRTEM image in (b) shows light regions which are consistent with low density regions, i.e. porosity in the film.

Figure 24 shows cross-section TEM images for Cu_2S films formed at low and high RH over the temperature range of 15°C to 35°C. TEM analysis reveals differences in grain sizes between low and high RH throughout the entire thickness of the Cu_2S layer, but does not reveal any significant difference in grain size at 15°C to 35°C for a given RH. Looking at these, we see

that the microstructure is not strongly dependent on temperature at a given RH. All of the low RH samples have large, columnar grains with well-defined grain boundaries, and all of the high RH samples have small, equiaxed grains with poorly defined grain boundaries. In addition, although we have shown that the rate of sulfidation at high RH changes once the Cu_2S layer reaches a thickness of about 150 nm, we see no evidence of a change in microstructure at any point in the Cu_2S layer. However, we see a clear difference in void concentration with temperature at high RH.

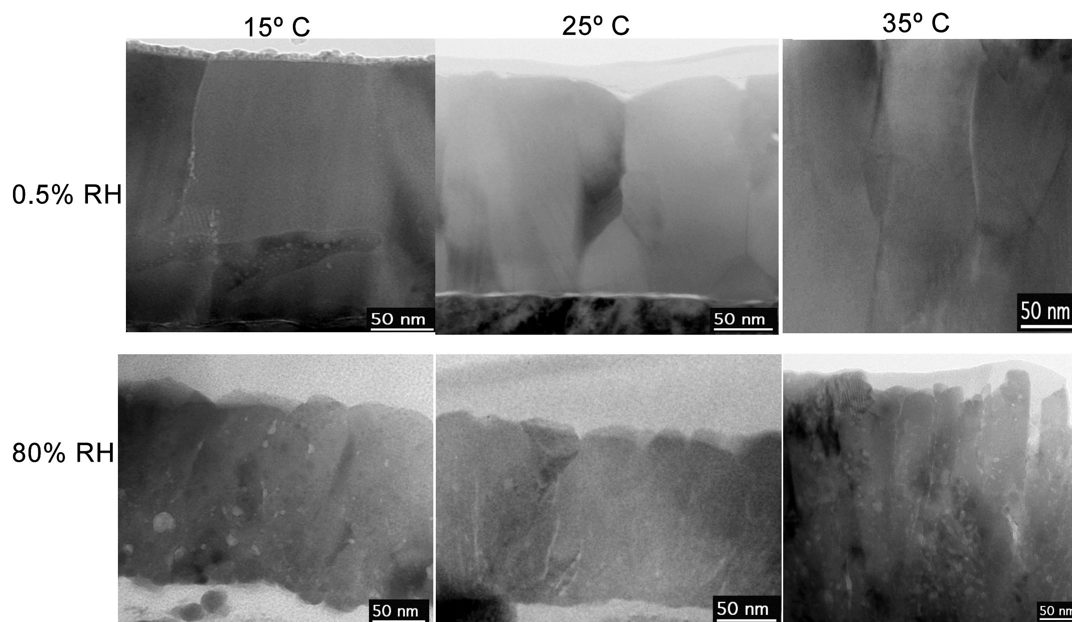

Fig. 24. Cross-section TEM images of Cu_2S films formed at low and high RH and a range of temperatures. For a given RH, the grain morphologies are similar with the low RH samples exhibiting large grains that span the film and the high RH samples exhibiting small grain sizes and high porosity.

A closer look at the porosity or void structure in the films grown at high RH is shown in Fig. 25. At 25°C the voids have coalesced along multiple grain boundaries to form long chains of voids, whereas at 35°C the voids appear to be greater in number and more spherical and more evenly distributed. The void concentration increases from about 2% (by volume) at 25°C to about 8% at 35°C.

Figure 26 shows a detailed analysis of the void structure for a Cu_2S film formed at high RH and 25°C. The HRTEM image in (a) shows both lattice fringes and void structure. A fast-Fourier transform (FFT) of the image was created, several sets of spots were selected, and an inverse FFT was performed. The resulting image is shown in (b). An outline of the void structure has been superimposed on the image to make its location more apparent. Upon comparing the original and processed image, we see that the voids appear to follow grain boundaries, one of which is indicated by an arrow. Based on the FFT analysis, there are no consistent lattice fringes observed in the void area, confirming that the voids represent a lack of Cu_2S as opposed to an alternative low density phase, such as $CuSO_4 \bullet H_2O$.

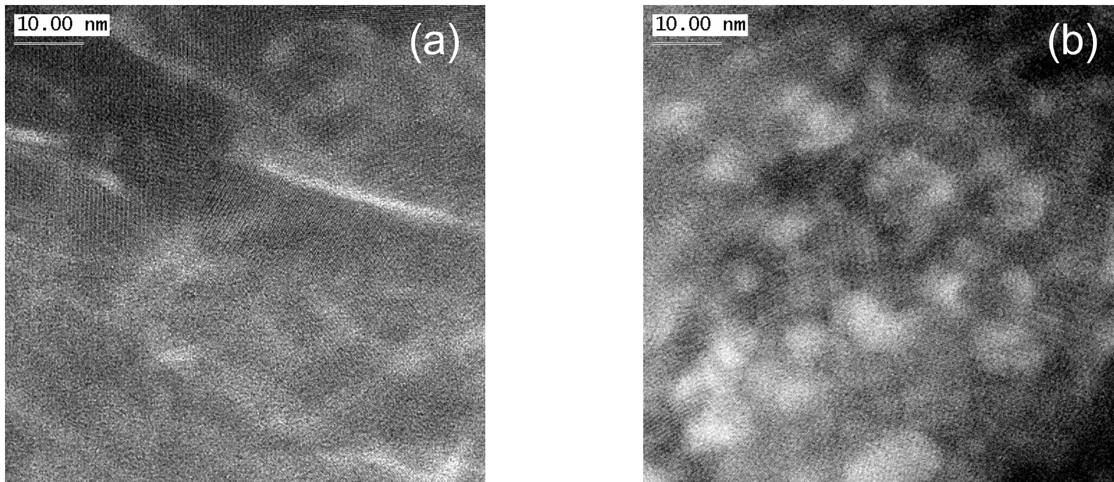

Fig. 25. HRTEM images of Cu_2S films formed at high RH at (a) 25 °C and (b) 35 °C. The images show an increase in porosity or void density with increasing sulfidation temperature. Also, the voiding is more equiaxed or spherical at higher temperature.

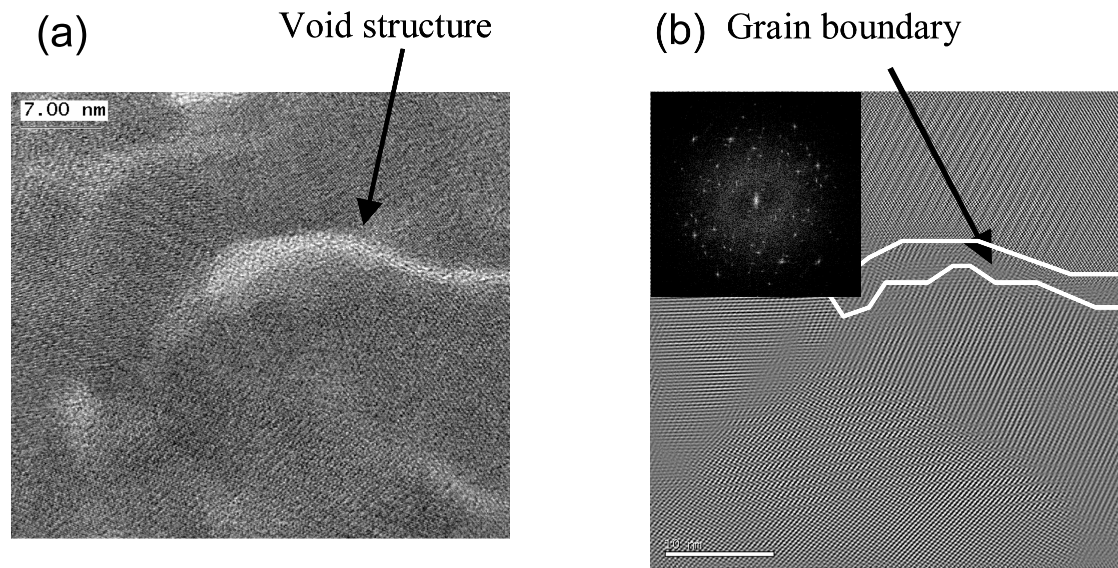

Fig. 26. HRTEM analysis of the void structure in a Cu_2S sample formed at high RH and 25 °C. An FFT analysis [inset in (b)] is used to identify all lattice fringes and the edges of grain boundaries. The void region is shown in the inverse FFT image in (b), and it corresponds to a region at the boundaries of the Cu_2S grains, implying that the grain boundaries have high void density.

The key observation from the TEM microstructural analysis is that there are gross microstructural differences in the Cu_2S films formed at low and high RH. The films formed at low RH show high quality crystalline grains and extensive grain growth with sulfidation time, suggesting solid phase epitaxy of new sulfide on to existing grains. These grains also apparently support a high flux of Cu during sulfidation (e.g. a high bulk diffusivity), otherwise, the sulfidation kinetics would show a decreasing rate with increasing sulfide thickness characteristic of solid state diffusion limited growth. In contrast, the Cu_2S films formed at high RH show

small Cu_2S grains with high void density at the grain boundaries. The leading speculation for the marked difference in grain morphology is that the sulfide grains formed at high RH may form from precipitation from the adsorbed H_2O layer that is present on the sulfide surface. (A thick adsorbed H_2O layer is not expected to be present at low RH.) This would explain the approximate uniform grain size which is independent of film thickness and the poor connectivity between grains as well as the random orientation of the grains.

The difference in grain morphology at high and low RH suggests a natural mechanism for the observed reduction in sulfidation rate at long times for films grown at RH. We attribute this to the poor connectivity between grains which inhibits the solid state transport of Cu through the Cu_2S layer. In essence, the hypothesized bottleneck is the inability for Cu to diffuse *between* grains of Cu_2S, and not the inability to diffuse Cu *within* grains. It is likely that the diffusion of Cu within the grains may still be rapid in the high RH samples, similar to what is seen in the low RH case (at least there is no data to contradict this). We also note that it is unlikely that grain boundary diffusion is fast in these films, at least for the high RH films, as the high RH films have far greater grain boundary area then the films formed at low RH, yet the apparent net diffusivity through the film is much less.

6.0 Diffusion Modeling

Based on the observation of the microstructures for the samples sulfidized at low and high RH, it is not surprising that Cu diffusivity through Cu_2S formed at high RH is much lower than the diffusivity in the low RH samples. One question which may be asked is whether the sulfidation kinetics observed in stage II growth at high RH (see Fig. 2) can be simply explained on the basis of a uniform low diffusivity through the Cu_2S layer. In this case, we would expect to see that the sulfide thickness increases with time with a $t^{1/2}$ dependence, and we should observe an activation energy which is characteristic for solid state diffusion, e.g. a few tenths of an eV. Figure 27 is a plot looking at the stage II kinetics for high RH sulfidation. A $t^{1/2}$ dependence was assumed for the non-linear region, and the slope was extracted in order to determine the activation energy for diffusion. As is shown in the Arrhenius plot, the data does not produce a clear activation energy for diffusion (the apparent activation energy would be close to zero). The reason for this is that diffusion through the Cu_2S is not expressed as uniform 1-D diffusion. A complete analysis of the stage II kinetics of sulfidation at high RH shows that the sulfidation rate slows down remarkably at long times, and even approaches zero. Again, this is in disagreement with a 1-D diffusion mechanism.

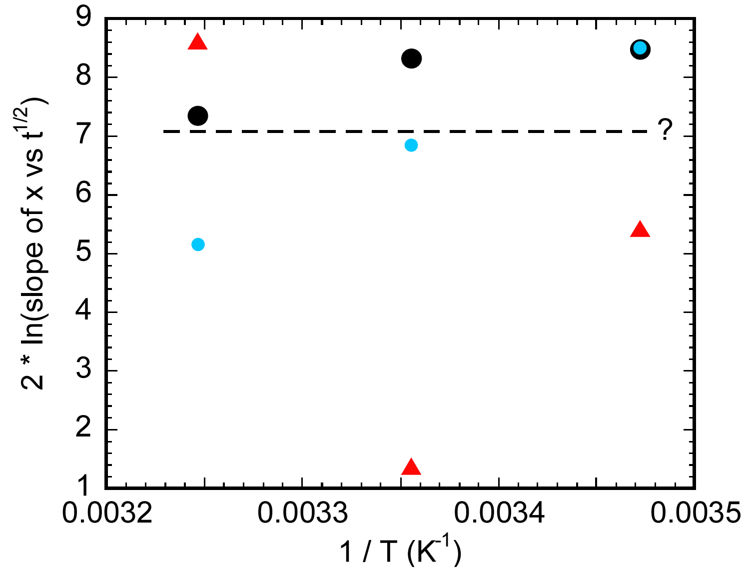

Fig. 27. Stage II kinetics of sulfidation at high RH are inconsistent with simple 1-D solid state diffusion limited growth, which would predict Cu_2S thickness with time increasing as $t^{1/2}$ and an activation energy characteristic of solid state diffusion, e.g. several tenths of an eV.

In order to understand the marked decrease in sulfidation rate at long times for high RH sulfidation, two-dimensional diffusion modeling was performed to determine whether the existence of localized source terms at the Cu/Cu_2S interface could be responsible for the suppression of Cu sulfidation at long times. The leading speculation is that the extensive voiding that exists at grain boundaries in the high RH material greatly reduces the flux of Cu between grains, leading to a reduction in the rate of sulfide film formation by an effect that can be modeled by a spatially limited source term for diffusion. To model this situation, a simulation was created in which there are line sources at the Cu/Cu_2S interface, and the effect of diffusion from these limited regions was calculated, see Fig. 28 [25]. The expected sulfide growth rate compared to the 1-D (planar source) is also shown in Fig. 28. The simulations show that the sulfidation rate is suppressed for source-limited diffusion; however, $t^{1/2}$ behavior would still be expected after long sulfidation times. From this, we conclude that the existence of static localized source terms would not result in the complete suppression of growth that is observed. However, if the sources become *increasingly* limited during sulfidation, i.e. the grains become increasingly poorly connected, then a continual reduction in sulfidation rate would be expected. A source term that becomes increasingly limited with time could be incorporated into new computational models for simulating copper sulfidation, and this is one of the principal suggested new directions for future research to follow on from this project.

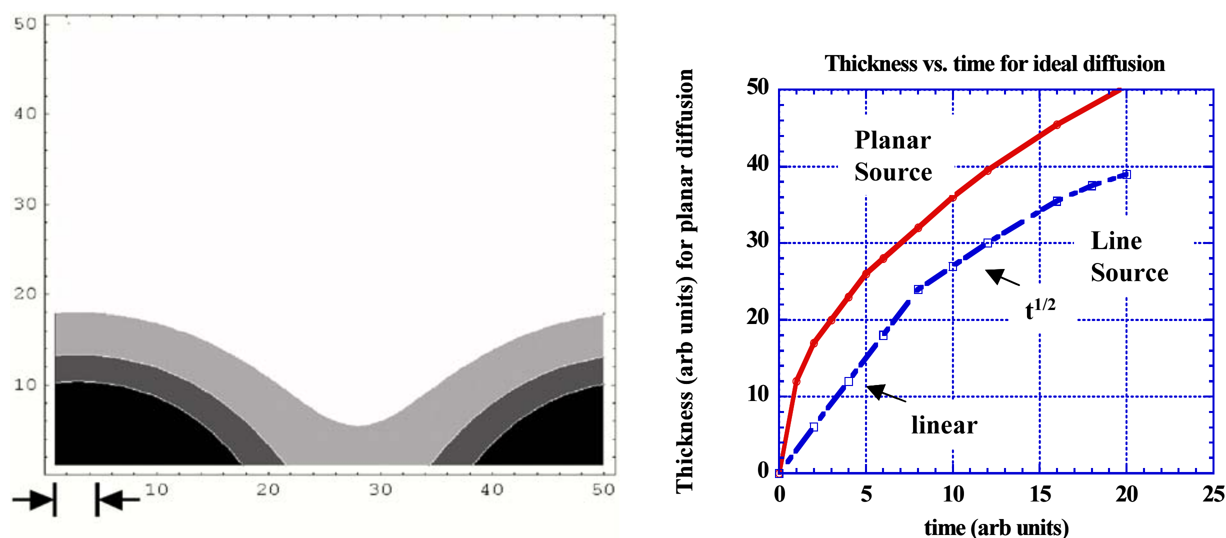

Fig. 28. 2-D computer modeling of Cu diffusion through Cu_2S. A limited source term (a line source) is assumed, as shown in the arrow-marked region of the contour plot on the left. The contours show the diffusion profile. The plot on the right shows the expected diffusion kinetics assuming a line source compared to the planar source. The plot shows that a decreased film thickness (lower sulfidation rate) would be expected for source-limited diffusion.

7.0 Summary

This project focused on developing understanding of the effect of relative humidity on copper sulfidation. The key question that was addressed is why the sulfidation kinetics at high RH are so different from the sulfidation kinetics at low RH. From studies of the initial stages of sulfidation, it was observed that nucleation of the sulfide is different at low RH compared to high RH, and the activation energy for sulfidation at low RH is characteristic of a surface-limited reaction while the activation energy for the initial stages of sulfidation at high RH is characteristic of a gas phase or liquid phase transport-limited reaction. Using specially-developed micro-test structures, it was shown that the ratio of the gas phase diffusivity to the surface reaction rate constant was between 10 and 100 for sulfidation at high RH. Finally, detailed experiments involving extensive high resolution transmission electron microscopy (HRTEM) revealed significant microstructural differences between Cu sulfides formed at low and high RH. TEM measurements of the Cu_2S morphology revealed that the Cu_2S formed at low RH has large sized grains (75 to greater than 150 nm) that are columnar in structure with sharp, abrupt grain boundaries. In contrast, the Cu_2S formed at high RH has small equiaxed grains of 20 to 50 nm in size. Importantly, the small grains formed at high RH have highly disordered grain boundaries with a high concentration of nano-voids. Further, different types of void structure were found as a function of temperature at the high relative humidity with room temperature sulfidation leading to elongated voids along grain boundaries and 35°C sulfidation giving a sponge-like microstructure of many small equiaxed voids. Thise difference in microstructure suggests that this could be the root cause of the different sulfidation kinetics at

high and low relative humidities. At low humidity, the sulfide layer forms much as if there is no impediment to the supply of copper whereas at high humidity the copper must diffuse through a tortuous path to reach the sulfidizing species. To examine this hypothesis in greater detail, simple diffusion modeling was performed using finite element analysis to simulate diffusion from a uniform planar front in comparison to diffusion from a front of distributed point sources (simulating the tortuous path/supply of Cu). The modeling indicated that the existence of static localized source terms would not predict the complete suppression of growth that was observed, but if the source terms became increasingly limited in time, due to increasingly poor connectivity between grains, then a source-limited diffusion process could be consistent with the experimental data.

In addition to the microstructural studies which formed the main part of this project, new micro-patterned test structures were developed. These electrical test structures were developed to measure the electrical conductivity of Cu_2S that forms on Cu. This information can be used to determine relative vacancy concentrations in the Cu_2S layer as a function of RH. The test structures involved micropatterned Cu disks and thin films, and the initial measurements showed that the electrical approach is feasible for point defect studies in Cu_2S.

8.0 Acknowledgments

The authors are indebted for experimental assistance in copper sulfidation, sample preparation, and experimental analysis by Jeff Braithwaite, Rob Sorensen, Sam Lucero, David Enos, Paula Provencio, Jim Mikkalson, Craig Johnson, Bill Breiland, and Bonnie McKenzie. In addition, the authors would like to thank Alan Wright, Harry Moffat, Amy Sun, Ken Chen, and Randall Cygan for their input on theory and simulation of Cu sulfides and Cu sulfidation. We would also like to thank Jane Zhu for technical advising. This work was supported by a Laboratory Directed Research and Development (LDRD) project at Sandia National Labs. Sandia is a multiprogram laboratory operated by Sandia Corp., a Lockheed Martin Co., for the U.S. Dept. of Energy's National Nuclear Security Administration under contract DE-AC04-94AL85000.

9.0 References

1. T. E. Graedel, K. Nassau and J. P. Franey, Corros. Sci. **27,** 639 (1987).

2. W. Wang, W. Langford and S. Muraka, Appl. Phys. Lett. **68**, 1622 (1996).

3. T. Do, S. Splinter, C. Chen and N. McIntyre, Surf. Sci. **387**, 192 (1997).

4. T. E. Graedel, J. P. Franey and G. W. Kammlott, Corros. Sci. **23**, 1141 (1983).

5. T. E. Graedel, J. P. Franey, G. J. Gualtieri, G. W. Kammlott and D. L. Malm, Corros. Sci. **25**, 1163 (1985).

6. T. E. Graedel, J. P. Franey, G. W. Kammlott, J. M. Vandenberg and P. L. Key, J. Electrochem. Soc. **134**, 1632 (1987).

7. S. P. Sharma, J. Electrochem. Soc. **127**, 21 (1980).

8. M. Watanabe, M. Tomita and T. Ichino, J. Electrochem. Soc. **148**, B522 (2001).

9. V. A. Phillips, J. Appl. Phys. **33**, 712 (1962).

10. U. Erb, H. Gleiter and G. Schwitzgebel, Acta. Met. **30**, 1377 (1982).

11. B. Chatlopadhyay and S. Sadigh-Esfandiary, Corros. Sci. **13**, 747 (1973)

12. M. Takeda, K. Fueki and T. Mukaibo, J. Electrochem. Soc. Jpn. **36**, 95 (1968).

13. C. Leygraf and T. E. Graedel in *Atmospheric Corrosion* (John Wiley and Sons, New York, 2000), p.44.

14. J. C. Barbour, J. W. Braithwaite and A. F. Wright, Nucl. Instr. Meth. Phys. Res., Sec. B, **175-177**, 382 (2001).

15. Jeff, Braithwaite, Sandia National Laboratories, private communication.

16. T. E. Graedel, Corros. Sci. **27**, 721 (1987).

17. B. J. Slatt, D. S. Natusch, J. M. Prospero and D. L. Savoie, Atmos. Environ. **12**, 981 (1978).

18. J. C. Barbour, J. P. Sullivan, M. J. Campin, A. F. Wright, N. A. Missert, J. W. Braithwaite, K. R. Zavadil, N. R. Sorensen, S. J. Lucero, W. G. Breiland, and H. K. Moffat, *"Mechanisms of Atmospheric Copper Sulfidation and Evaluation of Parallel Experimentation Techniques,"* SAND Report, SAND2002-0699 (2002).

19. A. Sun and H. Moffat, Sandia Memo on *"Parameter Estimation of Atmospheric Copper Sulfidation Corrosion Model,"* Jan. 29, 2003.

20. I. Grozdanov and M. Najdoski, J. Sol. State. Chem. **114**, 469 (1995).

21. Cu_2S PDF card no. 33-0490, International Center for Diffraction Data, Newton Square, PA.

22. A. F. Wright, Sandia National Laboratories, Albuquerque, NM, private communication.

23. M. J. Campin, J. G. Zhu, J. P. Sullivan, J. C. Barbour, J. W. Braithwaite, P. P. Provencio, Mater. Res. Soc. Proc. (J. C. Barbour, P. C. Searson, R. M. Penner, editors), 2003.

24. M. J. Campin, J. G. Zhu, J. P. Sullivan, J. C. Barbour, J. W. Braithwaite, and P. P. Provencio, to be submitted to J. Mater. Res. (2004).

25. M. J. Campin, *Microstructural Investigation of Copper Corrosion: Influence of Humidity*, Ph.D. Thesis, New Mexico State University (2003).

Distribution

Internal Distribution Only:

1	MS-0188	LDRD Office, 1011
3	MS-1421	John P. Sullivan, 1112
1	MS-1415	J. Charles Barbour, 1110
1	MS-1415	Nancy A. Missert, 1112
1	MS-1415	R. Guild Copeland, 1112
1	MS-1427	Julia M. Phillips, 1100
1	MS-9018	Central Technical Files, 8945-1
2	MS-0899	Technical Library, 9616